Title
Comparing the economic performance of ice storage and batteries for buildings with on-site PV through model predictive control and optimal sizing

Journal
Journal of Building Performance Simulation, 15(5)

ISSN
1940-1493

Authors
Hao, Kairui
Kim, Donghun
Braun, James E

Publication Date
2022-09-03

DOI
10.1080/19401493.2022.2084161

Peer reviewed

Comparing the Economic Performance of Ice Storage and Batteries for Buildings with On-site PV through Model Predictive Control and Optimal Sizing

Kairui Hao[a,*], Donghun Kim[b], James E. Braun[a]

[a] *School of Mechanical Engineering, Purdue University, West Lafayette, IN, USA*
[b] *Building Technology and Urban Systems Division, Lawrence National Berkeley Laboratory, CA, USA*

Abstract

Integrating renewable energy and energy storage systems provides a way of operating the electrical grid system more energy efficiently and stably. Thermal storage and batteries are the most common devices for integration. However, it is not clear which integrated storage system performs better in terms of overall economics. Ice storage has low initial and maintenance costs, but there is an efficiency penalty for charging of storage and it can only shift electrical loads associated with building cooling requirements. A battery's round-trip efficiency, on the contrary, is quite consistent and batteries can be used to shift both HVAC and non-HVAC loads. However, batteries have greater initial costs and a shorter life. This research presents a tool, using model predictive control and optimal sizing, and provides a case study for comparing life-cycle economics of battery and ice storage systems for commercial buildings that have chillers for cooling and an on-site photovoltaic system.

Keywords: ice storage, batteries, PV, thermal energy storage, model predictive control, optimal sizing, co-optimization

1. Introduction

The building sector has been the largest consumer of energy in the world over the past decades. Consequently, the utilization of on-site renewable energy resources combined with energy storage for buildings is seen as a powerful approach for mitigating energy consumption and accommodating demand response (DR). In order to induce end-users to manage their energy consumption behaviors wisely for the purpose of demand response, numerous utility companies offer time-dependent utility rate structures, which discourage on-peak electricity usage by employing time-of-use (TOU) energy cost rates and demand charges. Additionally, net energy metering (NEM) [1] as a renewable energy resources policy, which allows self-generated energy fed back into the grid with the same retail price, further incentivizes on-site distributed energy resource devices. Among all kinds of renewable energy technologies, installed photovoltaics (PV) capacity has shown a remarkable increase throughout the world in recent years. A PV system directly converts solar energy into DC electricity. This DC power could be directly used by DC apparatus or converted into AC power to

*Corresponding author
Email addresses: hao55@purdue.edu (Kairui Hao), donghunkim@lbl.gov (Donghun Kim), jbraun@purdue.edu (James E. Braun)

reduce the energy purchased from the utility grid. In order to optimize the daily utilization of a PV system that incorporates energy storage with variable utility rates, it is necessary to predict photovoltaic plant output power for different ambient conditions. The single diode model with five unknown parameters that can be estimated from manufacturers' data can be used to generate I-V characteristic curves of PV panel, [2] [3]. With variable electric rates, a stand-alone PV setup will not fully take advantage of the usage of solar-generated electricity without integration with energy storage. The most common ones are ice thermal storage and batteries. A natural question is which one will outperform the other in terms of economics for different situations.

Ice thermal storage has been demonstrated to perform well in terms of load shifting and peak demand shaving when TOU utility rate plans are incorporated. Many simple control strategies have been developed. Braun [4] and Drees and Braun [5] compared chiller priority, storage priority and optimal control strategies in terms of energy costs and demand charges and proposed a rule-based control strategy based on heuristics. The results show that under a favorable on-peak to off-peak cost ratio, a simple storage-priority strategy yields costs within 6% of optimal and significantly outperforms chiller-priority control. These simple control strategies could be easily implemented without a requirement of predictions of weather, occupancy and renewable energy information, etc.

In recent years, more sophisticated supervisory control [6] strategies have been developed that are able to systematically curtail energy and demand expenditures when combined with predicted information for systems with thermal storage. J. Candaned et.al [7] described a model-based predictive control (MPC) algorithm for the cooling plant of a building with ice storage under TOU utility rates. The method uses a simplified linear thermal model that is generated from a detailed building model in EnergyPlus. However, the MPC only focuses on minimizing energy costs and doesn't consider demand costs. Ma et.al [8] presented a complex MPC scheme that contains a high level MPC regulating the cooling plant with thermal storage and a low level MPC optimizing the operation of AHUs and VAV boxes. They pointed out a number of issues relating to this nonconvex MPC problem, e.g. stablity and feasibility, convergence to suboptimal solutions and computational complexity. Cox [9] proposed an approach that utilizes a neural network (NN) based model predictive control strategy that is solved by a genetic algorithm (GA) optimizer. Kircher and Zhang [10] formulated a convex optimization problem including uncertainties without consideration of demand charges. Tang et.al [11] studied MPC for phase change materials (PCMs) considering optimization of building demand response in smart grids. The author concluded that active thermal storage is necessary to ensure maintaining indoor temperature with further power reduction. Braun [12] systematically described a demand target reset algorithm that could handle a trade off between energy cost and demand charge in a suboptimal approach that could be implemented in practice.

As mentioned in [8], there are numerous issues when implementing an MPC controller in practice, including the trade off between model complexity and computational effort, and the possibility of local optimums. A model for a central cooling plant coupled with ice storage is highly nonlinear and also disjunctive due to different modes of operation for charging and discharging. A more elaborate system model can approximate real plant behaviors more precisely. However, a more complicated model is not only a computational burden, but also can deteriorate convergence to the global optimal solution. The references listed above either applied simple system models that don't consider system component capacity constraints that vary with operating conditions such that the optimal control input sequences could be solved with ease, or utilized detailed models that were solved with derivative-free optimization algorithms, e.g. particle swarm and genetic algorithms, which in general don't guarantee a global optimal solution. Lu et.al [13] developed a sophisticated plant model and compared the optimization results computed through mixed-integer nonlinear programming (MINLP) and nonlinear programming (NP). However, they didn't include demand charges and the optimization problem solver was not described explicitly. Vetterli and Benz [14] simplified a detailed

chiller model using a piece-wise linear function such that a mixed-integer linear programming could be derived as a computational simplification. However, they didn't construct a sufficiently detailed ice storage model that takes charging and discharging penalties into consideration[15].

The state of the art for battery technology enables the use of electric storage banks for both utility-scale and commercial building applications [16][17][18]. Rechargeable lithium-ion batteries are promising in a wide variety of fields due to their stable charging and discharging characteristics and high round-trip efficiency behavior[19]. Integrating batteries in systems with on-site PV could provide more design and control dimensions for managing energy demand response. Nottrott et.al [20] utilized linear programming (LP) to optimize grid-connected photovoltaic-battery storage system operation. They showed that the breakeven installed cost for a lithium-ion battery is about $400-$500 per kWh. Ranaweera and Midtgard [21] investigated the economic benefits when electricity can be sold back into the grid with consideration of the impact of reverse power flow. An adjustable, time-dependent grid feed-in power limit was introduced to handle the grid voltage stability issue occurring when a large amount of power is exported to the grid. Cai et.al [22] presented a model-based predictive control approach for operation of sustainable buildings with on-site photovoltaic and battery systems that balances building utility cost and battery life. In [23], a comprehensive multi-objective optimization problem was formulated that combines cases of fast charging with excess PV power, charging for maximizing battery lifetime, charging for maximizing self-consumption, charging for maximizing self-sufficiency and charging for cost minimization. This problem was solved by using dynamic programming (DP). Touretzky et.al [24] investigated economic MPC for buildings with chilled water storage. The TES model is a one-dimensional PDE and was discretized using a finite-difference approach.

Even though a large number of research publications were found that focused on optimal operation for central cooling plants coupled with ice thermal storage, and for PV systems integrated with battery storage, there appears to be very little literature on evaluating the economic performance when a central cooling plant system is integrated with on-site PV and different kinds of energy storage systems. Wang and Dennis [25] and Saffari et.al [26] explored the energy saving potential for an ice thermal storage coupled with PV. They concluded that when ice storage and solar PV are coupled together, further economic benefits could be achieved in comparison with using these two technologies independently. Savings attributed to PV only were primarily from energy cost savings, whereas the thermal storage could shift the on peak load and also improve the performance of off-grid solar PV system under variable PV generation conditions. Zhao et.al [27] studied the MPC problem for optimizing a solar PV-powered ice storage air conditioning system under forecast uncertainties. They used DP to minimize an objective function which does not include demand costs. Pandey et.al [28] performed a feasibility analysis of PV-Battery and PV-TES for cooling application in buildings. They studied two storage options, i.e., battery with PV and ice tank with PV, and concluded that energy storage self-consumption is higher for the PV-battery case compared to the PV-TES. However, they used simple models in the formulation of MPC, e.g., time-invariant equipment capacity constraints, and the objective function only considered minimization of the error between the controlled temperature and a reference temperature.

This paper develops optimal control and sizing methodologies and presents economic performance comparisons between two central cooling systems: 1) chiller plant + on-site PV + ice storage, and 2) chiller plant + on-site PV + battery storage (see figure 1(a), and 1(b)). In order to present a fair comparison between the systems coupled with thermal storage and electric storage, the sizes of chiller, PV and ice storage and control for each system were determined separately through life cycle cost minimization, termed co-optimal

design or just co-optimization where an optimal control problem is embedded in an optimal sizing problem.[1]. The present value of system costs was used as the metric which considers cash flows over the life cycle and aggregates them into the present value in order to give an investment evaluation. The life cycle economic performance for different systems depends on multiple elements such as the type of building, climate zone, utility rates, and renewable energy policies such that a simple conclusion cannot be derived. Hence a case study of a typical medium size commercial building in Riverside, California was analyzed as a guideline. Three common utility rate structures were considered: 1) time-of-use (TOU) energy with TOU demand charges; 2) TOU energy with any-time demand charges; and 3) only TOU energy charges. The situation is much more complicated when a demand charge exists since it incurs a trade off between a summation of energy costs and a single demand charge over a month. However, in practice it is not feasible to consider a monthly horizon for MPC due to prediction disturbances and heavy computational effort. Hence a demand limit reset algorithm was developed for MPC which converts the optimization problem into a short term horizon optimization problem. Net energy metering (NEM) is assumed that allows customers to sell back their self-generated distributive electric energy to the grid at the real-time retail price.

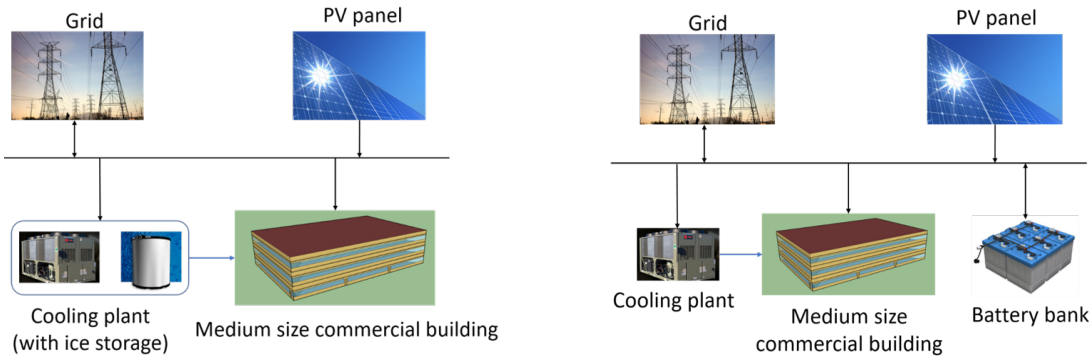

(a) On-Site PV coupled with Ice Storage

(b) On-Site PV coupled with Battery Storage

Figure 1: Schematic of system layouts

1.1. Technical contributions

In addition to the economic comparison between thermal and electric storages, our paper presents several technical methodologies from modeling, MPC formulation to algorithms to account for more physical constraints in the MPC formulation and to efficiently and reliably solve the co-optimal design problem with minimal simplifying assumptions. More precisely,

- A new grey-box modeling approach for ice-storage that combines physics with data to calculate variations on charging and discharging rates from the state-of-charge (SOC), storage-inlet water temperature and the corresponding water flow rate is proposed (see section 3.1.1).
- Our MPC problem accommodates a nonlinear performance map for chiller capacity, calibrated with manufacturer's data, in addition to a nonlinear chiller power map and physical capacity limits of the ice storage (see section 4.1).

[1]Note that the operating cost depends on a control strategy, and hence the control should also be optimized in addition to sizes of components to minimize the life cycle cost.

- A demand limit reset algorithm for the MPC is proposed to handle the long-term demand charge within the MPC framework (with a shorter, 1-day prediction horizon) and Dynamic Programming was utilized to ensure the global optimality for the complex MPC problem (see section 4.1 and 4.3).
- A sequential component sizing strategy is presented that aims to decouple the sizing process into two stages: sizing chiller and ice storage sizes by running the proposed MPC algorithm for ten-year life cycle simulations, and then sizing the PV or batteries using the annual electrical load profile obtained from the first stage (see section 5 and 5.2.2).

The technical advances in comparison to the literature with respect to modeling approaches for the cooling plant and energy storage, and types of MPC optimization problems are summarized in Table 1. It also indicates whether each paper focuses on the co-optimal design problem or only the optimal control problem (i.e., the utility cost minimization problem). There are several papers that solve the sizing problem without optimizing controls (by incorporating rule-based controls), e.g., [11; 24; 28–30], but those were not included in the Table.

In previous studies, dynamics of energy storage were mostly modeled with a simple energy balance and, for the ice-storage case, with models for the overall heat transfer coefficient (UA) between the ice and chilled water to capture charging and discharging constraints depending on the state of charge (SOC). However, none of the previous models accounted for the dependency on the water flow rate which could cause under or over-estimating the storage charging and discharging rates. For cooling plant modeling, despite a wide spectrum of chiller-power or COP modeling approaches, chiller capacity constraints were less strictly treated (mostly fixed capacity constraint). In addition, although many papers considered a demand charge, they treated it for the purpose of optimization-friendly formulation[2] not necessarily for the utility cost minimization. Finally, very few studies that investigate an approach to decouple the co-optimization problem were found.

[2]A typical approach to consider a peak demand in MPC replaces the maximum power or demand cost over a prediction horizon (in practice up to one or two days) with linear constraints and a slack variable, namely target peak or demand cost [31, Chapter 43]. This approach, however, is inconsistent with the way that actual demand charge is calculated because the target peak continuously varies for each time step for this approach.

Study	HVAC	TES/Battery type	Co-optimal design	Energy storage model /UA model for Ice-storage	Cooling plant model /Chiller capacity constraint	Demand consideration	MPC problem type /Solution approach	Decoupling approach
Drees and Braun [5]	Central plant	Ice storage	×	1d-energy balance /UA dependency on SOC	Nonlinear performance map/NA	✓	NLP/DP	NA
Candaned et.al[7]	Central plant	Ice storage	×	1d-energy balance /UA dependency on SOC	Nonlinear performance map /fixed capacity constraint	×	MINLP/YALMIP	NA
Ma et.al [8]	Central plant	Water tank	×	3d-moving boundary/NA	Nonlinear performance map /nonlinear capacity constraint	✓	NLP/NA	NA
Cox et.al [9]	Central plant	Ice storage	×	Neural network/NA	Neural network/NA	✓	MINLP/Genetic algorithm	NA
Kircher and Zhang [10]	Central plant	Ice storage	×	1d-energy balance/NA	Lack of detailed descriptions	×	Convex/Online tool	NA
Lu et.al[13]	Central plant	Water tank	×	Lack of detailed descriptions	Nonlinear performance map /fixed capacity constraint	×	MINLP/NA	NA
Cai et.al [22]	Central plant	Battery	×	1d-energy balance/NA	Nonlinear performance map /fixed capacity constraint	✓	Convex/CVX MATLAB	NA
Saffari et.al [26]	Central plant	Generic TES	×	1d-energy balance/NA	Constant COP model /fixed capacity	✓	MILP/NA	NA
Zhao et.al [27]	Central plant	Ice storage	×	1d-energy balance /Constant UA	Nonlinear performance map /fixed capacity constraint	×	Stochastic/DP	NA
Meyer & Emery [32]	Central plant	Ice storage	✓	1d-energy balance/NA	Nonlinear performance map /fixed capacity constraint	✓	NLP/DP	×
Vetterli & Michael [14]	Central plant	Ice storage	✓	1d-energy balance/NA	Piecewise linear COP /linear capacity constraint	✓	MILP/CPLEX	×
Baniasadi et.al.[33]	Central plant	Water tank battery	✓	2-d moving boundary/NA	Carnot COP model/NA	×	NLP/Particle Swarm	×
Urbanucci et.al. [34]	Combined Heat & Power	Water tank	✓	1d-energy balance/NA	NA (heating)	×	MILP/CPLEX	×
Chen et.al. [35]	Central plant	Ice storage	✓	1d-energy balance /UA dependency on SOC	Nonlinear power map /fixed capacity constraint	×	NLP/DP	×
This paper	Central plant	Ice storage battery	✓	1d-energy balance /UA dependency on SOC and flow rate	nonlinear performance map /nonlinear capacity constraint	✓	NLP/DP	✓

Table 1: Summary of studies on optimal control and co-optimization for cooling TES/battery plants

2. Case study description

2.1. Site description

The case study used Riverside, California as the location with meteorological data extracted from the Typical Meteorological Year (TMY3) data set. Its latitude is 33.95 N and longitude is 117.38 W. This is a hot semi-arid climate with hot summers and warm to cool winters, and with minimal precipitation. The location was chosen to minimize the influence of heating on the overall economic performance evaluation. In order to have a fair comparison between thermal storage and electric storage, it was assumed that both systems use natural gas for heating. If a heat pump for heating were utilized, batteries could play a load shifting role whereas the ice storage could not.

2.2. Building model

A medium size commercial building model was extracted from the EnergyPlus prototypical building library[36] and all the parameters were set as default. The building has three floors with 53,600 sq feet of floor area. Windows are evenly distributed along four facades with a 33% window fraction. The detailed setup for the architecture, interior loads and schedules were unchanged. An annual building cooling load profile (HVAC load) and electric loads associated with other devices (non-HVAC loads) were computed and used as inputs to an optimal component sizing platform, and simulation testbed that incorporated an MPC algorithm. The maximum cooling load occurs on September 11th which is 226kW and the design day total cooling load is 2836.75 kWh.

2.3. Utility rate plan

The utility rate plays the most decisive role in affecting the economic benefit of integrating energy storage into the system in this case study. In this study, three representative California TOU rates were chosen that are summarized in table 2. Demand costs were determined based on 1 hour average power and TOU energy costs were charged based on 15-minute energy flows. The utility rate PG&E A10 has an any-time demand charge which might cause the cost saving coming from demand charges by load shifting to be small. However the on-peak to off-peak energy rate ratio in summer is about 1.6 which is the primary cost saving potential driver. The utility rate SCE GS-2B also has a significant on-peak to off-peak energy cost ratio in summer of 2.1, and also has a TOU demand cost rate. SCE GS-R is quite different in that it doesn't have a demand charge. However its on-peak to off-peak energy cost ratio is about 5.5 providing a significant incentive for use of storage.

2.4. Net energy metering

The Net Energy Metering 2.0 (NEM) is an established policy in California that is continually adapted. Customers with eligible renewable generation facilities installed behind the customers' meters that meet technical requirements are able to participate in the NEM tariff.

Under NEM, customer-generators offset their charges for any consumption of electricity provided directly by their renewable energy facilities and receive a cumulative financial credit monthly for the power generated by their on-site renewable energy systems that is fed back into the power grid for use by other utility customers over the course of a billing cycle. The unique speciality of NEM is that the credits are valued at the same price that customers would otherwise be charged for electricity consumed. At the end of every year that a customer-generator has been on the NEM tariff, the credits and charges accrued over the previous 12-month billing period are "trued-up".

In this study, we assumed that any excess generated energy at the end of the billing year was wasted. Other fees associated with the NEM program enrollment, such as interconnection fee and non-bypassable

Table 2: TOU utility rate plans

TOU Energy Rate ($/kWh)						
	PG&E A10		SCE GS-2B		SCE GS-R	
Summer	On-Peak	0.22455	On-Peak	0.12280	On-Peak	0.39056
	Partial-Peak	0.16942	Partial-Peak	0.08040	Partial-Peak	0.13509
	Off-Peak	0.14135	Off-Peak	0.05772	Off-Peak	0.0707
Winter	Partial-Peak	0.14107	Partial-Peak	0.07664	Partial-Peak	0.08962
	Off-Peak	0.12400	Off-Peak	0.06514	Off-Peak	0.07812
Demand Charge Rate ($/kW)						
	PG&E A10		SCE GS-2B		SCE GS-R	
Summer	Any-time	19.13	On-Peak	19.61	Any-time	0
			Partial-Peak	3.83		
			Off-Peak	0		
Winter	Any-time	11.24	Any-time	0	Any-time	0

charges were assumed to be small and the same for all cases, thus were not considered in the formulation of the optimization problem.

2.5. Life cycle financial performance metric

In this study, we selected the Present Value as the metric to evaluate the life cycle cost performance of different systems coupled with ice storage or batteries. The Present Value is a straightforward variable that aggregates cash flows happening during the course of a time-line in the future that investors are interested in. The Present Value of system costs is calculated based on equation 1.

$$SC_{PV} = \sum_{t=1}^{n} R_t \left(\frac{1+i}{1+d}\right)^t + C_{ii} \tag{1}$$

where R_t is the system operation and maintenance costs during a single period t, i is the annual inflation rate, d is the discount rate, n is the number of time periods and C_{ii} is the initial investment. The parameter values to be considered, referring to [37] and [38], in this study are listed in table 3.

Table 3: Present value parameter assumption

Parameter	Value
i	2%
d	7%
n	10

2.6. Installed costs of system components

The installed cost of the system either coupled with ice storage or batteries is a pivotal factor that determines not only the sizing but also the overall life cycle cost. Therefore it is an essential and fundamental parameter in the study. For the chiller and ice storage, the installed prices are quite stable and low compared

with batteries. In contrast, the costs of renewable energy such as photovolotaics and the associated battery storage are varying significantly in recent years. Consequently, the current installed costs are used as a benchmark followed by a parametric study of installed cost values in the study.

The installed cost of cool thermal energy storage used in this study is based on a report[39] published in 2006 . The installed cost estimates were adjusted to today's costs assuming an annual inflation rate of 7 %. The storage medium of this study is ice on coil, internal melt. Thus the installed cost of a chiller and ice storage were chosen as the mean value of each cost range, i.e. 735 $/ton for a chiller and 126 $/ton-hour for an ice tank.

The installed costs for batteries depend on the battery material, battery power capacity and battery energy storage capacity. Battery power capacity and battery energy storage capacity can be represented by a single parameter called duration, which is the ratio of energy storage capacity to power capacity. The classification of battery storage duration is short duration (<0.5 hours), medium-duration (0.5∼2 hours) and long-duration (>2 hours). For cost information we referred to a report from the National Renewable Energy Laboratory[16]. This paper assumes lithium-ion batteries because of their stable and reliable operation characteristics. For a commercial building scale Li-ion storage system (10∼1000kW), batteries should be classified as long-duration storage. Batteries installed cost consists of two parts which are energy capacity cost ($/kWh) and power capacity cost ($/kW). For a 2-hour duration battery, the energy capacity cost was assumed to be 454 $/kWh.

Solar photovoltaic (PV) deployment has grown rapidly in the United States over the past several years due to the rapid decreasing initial cost. The dramatic cost drop makes the application of PV for distributed generation more intriguing and promising at present and in the future. The installed cost was taken to be 1.88 $ per peak watt [17].

A summary of system components installed costs is shown in table 4.

Table 4: System components installed cost estimates

System component	Chiller	Ice storage tank (Ice on coil, internal melt)	Li-ion battery (0.5 C-rate)	Solar PV
Installed cost estimate	421-1052 $/ton	105-147 $ /ton-hour	454 $/kWh	1.88 $/W

2.7. Maintenance costs

Since the economic performance only considers a ten-year time horizon, this study only includes maintenance costs without replacement. The maintenance costs for the PV system are taken to be 18 $/kW per year, which means the overall maintenance costs for ten years are about 10% of the PV installed cost[17]. For lithium-ion batteries, the maintenance costs are taken to be 7.8 $/kW per year[16], which could be converted to 3.9 $/kWh per year with a 0.5 C-rate. This corresponds to maintenance costs for lithium-ion batteries of about 8.6% of their installed cost in terms of a ten-year operating duration. The maintenance cost of a cooling plant is considered as 2% of the installed cost.

3. Development of simulation testbed for central cooling system with ice storage and batteries

3.1. Central cooling system modeling

This section describes the central cooling plant system configuration and component models used in this work. A series configuration with chillers being upstream of storage shown in figure 2 is considered throughout this research since it allows the chiller to operate at a relatively higher evaporating temperature

for a higher COP. The baseline system for the case study has a 52-ton air-cooled chiller with 30% propylene glycol and 70% water in the circulating loop, 4 single-stage scroll compressors, two refrigeration circuits and two 250 ton-hour identical ice tanks. In this study, the baseline component capacities are scaled according to sizing specifications based on loads and economic considerations.

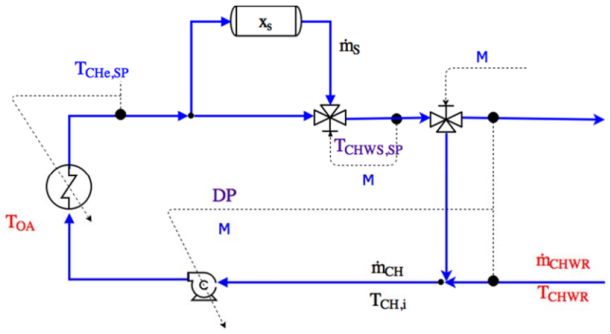

M: plant modes (off, chiller only, ice only, chiller and ice, freezing)
DP: pressure differentials
T_{OA}: outdoor dry bulb temperature
$T_{CHe,SP}$: chiller exit temperature setpoint
$T_{CHWS,SP}$: primary chilled water supply temperature setpoint
$T_{CH,i}$: chiller inlet temperature
T_{CHWR}: return water temperature from building
$\dot{m}_s$: mass flow rate passing two ice storage tanks
$\dot{m}_{CH}$: mass flow rate passing chiller
$\dot{m}_{CHWR}$: mass flow rate from building
$\dot{x}$: ice storage state of charge

Figure 2: Schematic of ice storage chiller plant and nomenclature

3.1.1. Ice storage model

In this study, ice tanks utilized an internal-melt, ice-on-coil configuration. For this type of ice storage device, we refer to the semi-empirical model developed by West and Braun (1998) with modifications explained as follows. The maximum discharging and charging rates (positive for discharging and negative for charging) can be expressed as:

$$Q_{IS} = \epsilon_D(x_s, \dot{m}_s)\dot{m}_s C_{p,w}(T_{s,i} - T_{fr}) \quad (T_{s,i} > T_{fr}) \tag{2}$$

$$Q_{IS} = \epsilon_C(x_s, \dot{m}_s)\dot{m}_s C_{p,w}(T_{s,i} - T_{fr}) \quad (T_{s,i} \leq T_{fr}) \tag{3}$$

where $T_{s,i}$ is the water/glycol mixture fluid ice storage inlet temperature (also the chiller outlet temperature), T_{fr} is the freezing point temperature (0°C for water), $\dot{m}_s$ is the mass flow rate passing two ice storage tanks, $C_{p,w}$ is the specific heat of water/glycol mixture fluid, ϵ_D and ϵ_C are the heat transfer effectiveness for discharging and charging which are a function of the state of charge (x_s) and mass flow rate ($\dot{m}_s$). The storage model neglects any heat gains through the storage shell and treats the storage as a lumped system whose state can be denoted by a single variable, i.e., state of charge (SOC), which is defined as:

$$x_s = \frac{u_f - u_{IS}}{u_{sf}} \tag{4}$$

where u_{IS} is the specific internal energy of the water and ice mixture in the tank, u_f is internal energy of saturated liquid water, and u_{sf} is the latent heat of fusion for ice. Hence the energy balance of ice storage is given by equation 5, where C_s is the total ice storage capacity.

$$\dot{x}_s = -\frac{Q_{IS}}{C_s} \tag{5}$$

Combining equation 2, 3 and 5 leads to a lumped dynamic model of ice storage in equation 6 and equation 7.

$$\dot{x}_s = \frac{\epsilon_C(x_s, \dot{m}_s)\dot{m}_s C_{p,w}(T_{fr} - T_{s,i})}{C_s} \quad (T_{s,i} \leq T_{fr}) \tag{6}$$

$$\dot{x}_s = \frac{\epsilon_D(x_s, \dot{m}_s)\dot{m}_s C_{p,w}(T_{fr} - T_{s,i})}{C_s} \quad (T_{s,i} > T_{fr}) \tag{7}$$

The two dynamic equations require a model for heat transfer effectiveness during charging and discharging. We adapted the approach presented by West and Braun (1999) which uses a polynomial to correlate charging and discharging effectiveness with the state of charge at a fixed flow rate using experimental data. The charging and discharging heat transfer effectiveness regression representations for a fixed flow rate with each 250 ton-hour ice storage tank at 4.4877 kg/s (57.4 gpm) are given in equations 8, where the subscripts denote that the charging and discharging heat transfer effectiveness are tuned for a fixed flow rate $\dot{m}_{0,s}$.

$$\begin{aligned} \epsilon_{0,C}(x_s) &= -8.5333x_s^5 + 14.8774x_s^4 - 8.4289x_s^3 + 1.3921x_s^2 - 0.2911x_s + 0.9839 \\ \epsilon_{0,D}(x_s) &= 19.9760x_s^5 - 56.1250x_s^4 + 58.9749x_s^3 - 28.2980x_s^2 + 6.3670x_s + 0.1217 \end{aligned} \tag{8}$$

With these two polynomial regression models tuned for a fixed experimental mass flow rate data set, we propose to extract the heat transfer effectivenesses for charging and discharging at different mass flow rates in the following manner and we drop the subscripts C and D.

We start with the following model structure.

$$\epsilon(x, \dot{m}_s) = 1 - e^{-\frac{(UA)(x)}{\dot{m}_s C_{p,w}}} \tag{9}$$

At a given state, the relationship should hold since the the ice-storage temperature is maintained during charging and discharging processes. The function, $(UA)(\cdot)$, describes how the thermal resistance between the chilled water and ice storage varies depending on the formation or melting of ice. The $\epsilon - NTU$ model structure provides a way of retrieving the functional forms of (UA) from the dataset measured at the fixed flow rate. The detailed steps are as follows,

With the tuned ϵ_0 at the given flow rate $\dot{m}_{0,s}$, from equation 9, we can express (UA) as,

$$(UA)(x) = -\dot{m}_{0,s} C_{p,w} ln(1 - \epsilon_0(x)) \tag{10}$$

then substitute 10 into 9 to derive the functional form of $\epsilon(x, \dot{m}_s)$,

$$\epsilon(x, \dot{m}_s) = 1 - (1 - \epsilon_0(x))^{(\dot{m}_{0,s}/\dot{m}_s)}. \tag{11}$$

To validate this modeling approach, experimental data from [40] was used and comparisons with good agreement are shown in Fig. 3(a) and 3(b).

3.1.2. Air-cooled chiller model

A chiller model was obtained by regression using manufacturer's data for a 52-ton chiller having 4 compressor stages. Open-loop and closed-loop models were developed. The open-loop model means there is no control of the chiller outlet temperature setpoint and the compressor stage is an input. For this model, the maximum chiller capacity and corresponding power are a function of chiller inlet temperature ($T_{CH,i}$), brine mass flow rate ($\dot{m}_{CH}$), ambient dry bulb temperature (T_{OA}) and compressor stage.

$$\begin{bmatrix} Q_{CH,max} \\ P_{CH,max} \end{bmatrix} = f_{OL}(T_{CH,i}, \dot{m}_{CH}, T_{OA}, Stage) \tag{12}$$

The closed-loop model is applied to the case where the chiller outlet temperature is controlled to its setpoint ($T_{CHe,SP}$) through control of the compressor stage.

$$P_{CH} = f_{CL}(Q_{CHL}, T_{CHe,SP}, T_{OA}) \tag{13}$$

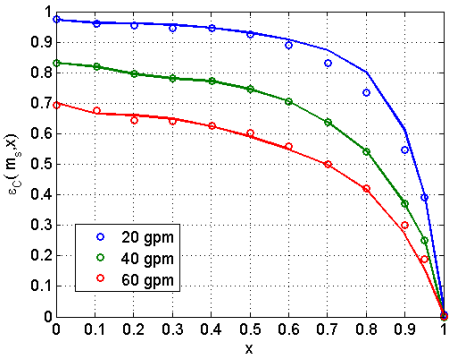

(a) Comparison of model predictions (solid lines) and experimental results (dots) during charge

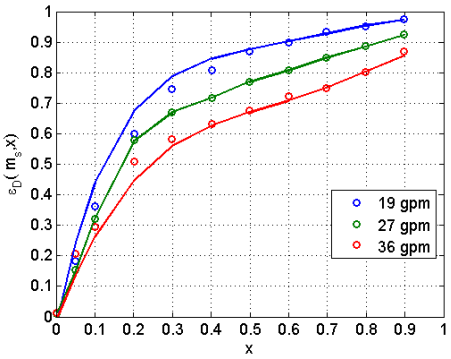

(b) Comparison of model predictions (solid lines) and experimental results (dots) during discharge

Figure 3: Validation of the ice storage charging and discharging heat transfer effectiveness model

The open loop chiller model with stage equal to max stage gives maximum chiller cooling capacity which is used as a constraint in the optimization problem formulation, whereas the closed loop chiller model describes the required power to meet a chiller outlet temperature setpoint. Equations 14-16 are second-order polynomials that were determined through least-squares regression (the regression approach for chiller performance mapping is the standard method used in, e.g., DOE2 and EnergyPlus [41]), and the validation results are presented in figure 4.

$$Q_{CH,max} = 87.4537 + 4.1228T_{CH,i} + 11.1804\dot{m}_{CH} + 0.2256T_{OA} + 0.0194T_{CH,i}^2 - 0.4630\dot{m}_{CH}^2 - 0.0153T_{OA}^2 + 0.1293T_{CH,i}\dot{m}_{CH} - 0.0390T_{CH,i}T_{OA} - 0.0663T_{OA}\dot{m}_{CH} \tag{14}$$

$$P_{CH,max} = 30.6853 + 0.1525T_{CH,i} + 0.7983\dot{m}_{CH} + 0.2208T_{OA} + 0.0024T_{CH,i}^2 - 0.0396\dot{m}_{CH}^2 + 0.0108T_{OA} + 0.0105T_{CH,i}\dot{m}_{CH} + 0.0049T_{CH,i}T_{OA} + 0.0009T_{OA}\dot{m}_{CH} \tag{15}$$

$$P_{CH} = 2.2586 + 0.1737Q_{CHL} + 0.0138T_{CHe,SP} - 0.3455T_{OA} + 0.0001Q_{CHL}^2 + 0.0123T_{CHe,SP} + 0.0096T_{OA}^2 - 0.0063Q_{CHL}T_{CHeS,P} + 0.0056Q_{CHL}T_{OA} - 0.0103T_{CHe,SP}T_{OA} \tag{16}$$

3.1.3. Pump model

In this study, a simple empirical model was employed that relates pump power consumption to flow rate:

$$P_{\text{pump}} = \frac{V_f(DP)}{\eta_{\text{pump}}\eta_{\text{motor}}\eta_{\text{inverter}}} \tag{17}$$

where V_f is volume flow rate (m^3/s), DP is the pressure difference between supply and return pipes, η_{pump} is the pump efficiency, η_{motor} is the motor efficiency, and η_{inverter} is the inverter efficiency. Pressure differences primarily depend on the chiller mode and were obtained from manufacturers' data. The DP of "Off",

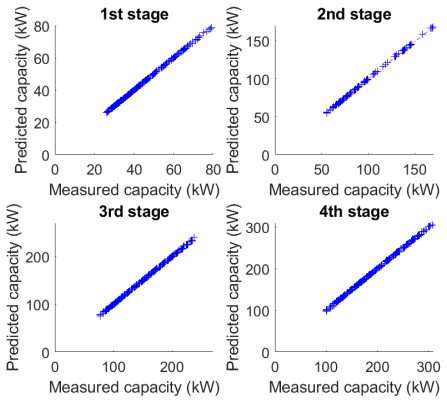

(a) Open loop chiller capacity

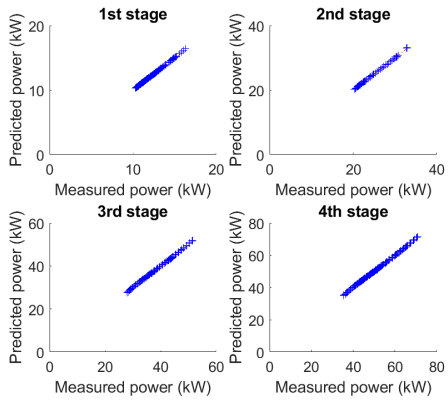

(b) Open loop chiller power

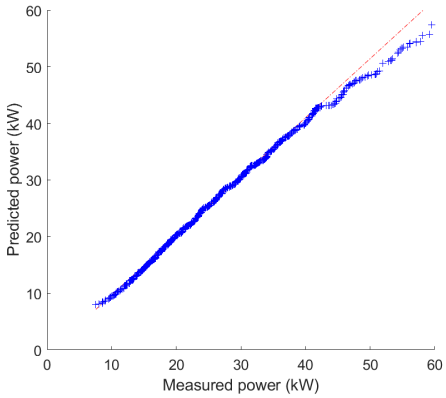

(c) Closed loop chiller power

Figure 4: Validation of the chiller second-order polynomials models

"Chiller only", "Ice storage only", "Chiller and ice storage", "Freezing" are 0, 44.7, 85.4, 43.8 and 34.1 kpa, respectively. η_{pump}, η_{motor} and η_{inverter} are 0.4, 0.9 and 0.95, respectively, which also were obtained from manufacturers' data.

3.1.4. Central cooling plant modeling

The central cooling plant model for the system coupled with ice storage is more complicated than the system coupled with batteries since there are five plant modes in total: "Chiller plant off (OFF)", "Chiller only (CH)", "Ice cooling (discharging) only (I)", "Chiller and Ice cooling (CHI)" and "Freezing (charging) ice (F)". A mode where the chiller meets the cooling load and charging storage at the same time ("Chiller and Freezing") is not considered due to low COP and high operating cost. For the system coupled with battery storage, only modes "Chiller plant off (OFF)" and "Chiller only (CH)" are considered.

The plant model predicts outputs and states according to cooling load (CWL), outdoor dry bulb temperature (T_{OA}) and other parameters and conditions with control decisions of chiller outlet temperature

setpoint ($T_{CHe,SP}$) and plant modes (M). The overall plant model has the following discrete time form:

$$\begin{aligned}\left[x_s(k+1), y(k)\right] &= f_{plant}\left(x_s, T_{CHe,SP}, M, \dot{m}_{CHWR}, CWL, T_{OA}, T_{CHWS,SP}, DP, Maxstage, \Delta t\right)_k \\ y(k) &= \left[T_{CH,i}, T_{CH,e}, T_{s,e}, \dot{m}_s, Q_{CH}, Q_{CHL}, Q_{CH,max}, P_{CH}, Q_{IS}, Q_{ISL}, Q_{IS,max}, P_{pump}\right]_k\end{aligned} \quad (18)$$

where Q_{CH} is the chiller cooling capacity, Q_{CHL} is the chiller cooling load to meet $T_{CHe,SP}$, and $Q_{CH,max}$ is the maximum chiller capacity defined as the heat transfer rate from water/glycol to the chiller with full stage compressors. Q_{IS} is the ice storage cooling capacity defined as the heat transfer rate from water/glycol to the tank, Q_{ISL} is the ice storage cooling load which is the required heat transfer rate to meet a given setpoint for the primary supply water temperature, and $Q_{IS,max}$ is the maximum ice storage capacity that occurs when the mixing valve of the tank is fully open to the tank when all of mass flow goes through ice storage. $T_{CH,e}$ is the chiller outlet temperature and $T_{s,e}$ is the ice storage outlet temperature. Cooling loads, capacities and maximum capacities are distinguished in the model for cases where the chiller and ice storage do not have enough capacities to meet their loads. When they are able to meet their loads, cooling capacities are equal to cooling loads.

3.2. Battery storage and photovoltaics modeling

3.2.1. Battery model

The battery dynamics can also be approximated by the concept of state of charge:

$$x_b(k+1) = x_b(k) - \frac{I(k)\Delta t}{Q_{bat,I}} \quad (19)$$

where I (Amp) is the current and positive for discharging and negative for charging, $Q_{bat,I}$ (Amp-hr) is the battery current capacity and Δt is the time step. A detailed lithium-ion battery model from MATLAB Simulink Electric Drives/Extra Sources library was used to obtain a linearly interpolated battery model based on a typical battery's charging and discharging characteristics.The inputs of the MATLAB Simulink lithium-ion battery model are discharging (charging) current ($I(k)$), initial state of charge ($x_b(k)$) and simulation time duration (Δt). The outputs are voltage (V) and state of charge (x_b) variations from time $k\Delta t$ to $(k+1)\Delta t$. By integration of voltage and current, battery averaged discharging and charging power over time duration (Δt) can be computed. The overall linearly interpolated battery model has the form in equation 20.

$$\begin{bmatrix} x_b(k+1) \\ P_b(k) \end{bmatrix} = F(I(k), x_b(k), \Delta t) \quad (20)$$

where $P_b(k)$ represents the averaged battery power over time Δt. For the model predictive control algorithm, Δt is one hour and for the system simulation testbed Δt is 15 minutes. To prevent low and high states of charge, the state of charge is subjected to the constraint in equation 21.

$$0.25 \leq x_b(k) \leq 0.95 \quad (21)$$

3.2.2. Photovoltaics model

A photovoltaic system converts sunlight into DC electricity that can be used on site or support other grid users when extra generated electricity is available. The fundamental element is a PV cell which can be grouped into PV panels and arrays. A single diode model of a PV cell (figure 5)[2] was utilized in this study to obtain a photovoltaic output power profile. I_{pv} is the current generated by the incident light, I_d is the

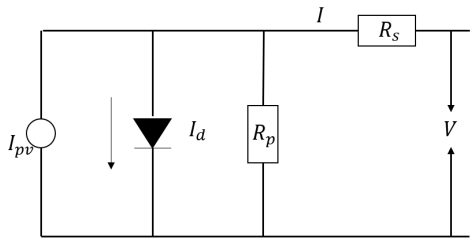

Figure 5: schematic of single-diode model of PV cell

Shockley diode equation 22, R_s is the equivalent series resistance of the module and R_p is the equivalent parallel resistance.

$$I_d = I_{0,cell}(e^{\frac{V_D}{V_t}} - 1) \tag{22}$$

where I_d is the diode current, $I_{0,cell}$ is the reverse saturation current, V_D is the voltage across the diode, and V_t is the thermal voltage defined as $V_t = \frac{AkT}{q}$. A is the ideality factor, k is the Boltzmann constant, T is the diode temperature, and q is the electron charge.

The solution of the equation for this model leads to an $I - V$ relation for the PV module that has the form in equation 23.

$$I = I_{PV} - I_0[e^{\frac{V+R_sI}{N_sV_t}} - 1] - \frac{V + R_sI}{R_p} \tag{23}$$

where I_{PV} ($I_{PV} = I_{PV,cell}N_P$) is photovoltaic current of the photovoltaic module, I_0 ($I_0 = I_{0,cell}N_P$) is the saturation current of the photovoltaic module, N_p is the number of cells connected in parallel to increase output current and N_s is number of cells connected in series to give the desired output voltage. Equation 23 results in an $I - V$ curve which represents characteristics of a PV module. Three remarkable points in $I - V$ curve are the short circuit $(0, I_{sc})$, maximum power(V_{mpp}, I_{mpp}) and open circuit points $(V_{oc}, 0)$[2].

There are five unknowns in equation 23 which are I_{PV}, I_0, R_s, R_p and A to be determined in order to obtain an $I - V$ relation. For parameters R_s,R_p and A, an approach that refers to the manufactures' datasheet was utilized to compute them. Typically, the parameters provided from the data sheet are I_{sc}, V_{oc}, V_{mpp}, I_{mpp}, P_{mpp}, k_i and k_v, where P_{mpp} is the maximum power, k_i is the temperature coefficient of I_{sc}, and k_v is the temperature coefficient of V_{oc}. The standard test condition (STC) means an irradiation of 1000W/m^2 with an AM1.5 spectrum at 25°C, where AM1.5 means that air mass coefficient is 1.5 (The air mass coefficient defines the direct optical path length through the Earth's atmosphere, expressed as a ratio relative to the path length vertically upwards, i.e. at the zenith). By substituting data for current and voltage at the three known points (the short-circuit, maximum power and the open-circuit points) into the $I - V$ equation, then the following three equations can be derived[2].

$$\begin{aligned}
I_{sc} &= I_{PV} - I_0 e^{\frac{I_{sc}R_s}{n_sV_t}} - \frac{I_{sc}R_s}{R_p} \\
I_{mpp} &= I_{PV} - I_0 e^{\frac{v_{mpp}+I_{mpp}R_s}{n_sV_t}} - \frac{V_{mpp} + I_{mpp}R_s}{R_p} \\
I_{oc} &= 0 = I_{PV} - I_0 e^{\frac{V_{oc}}{n_sV_t}} - \frac{V_{oc}}{R_p}
\end{aligned} \tag{24}$$

For I_{PV}, the photovoltaic current depends linearly on the solar irradiation and is also influenced by the temperature according to equation 25:

$$I_{PV} = (I_{PV,n} + k_i \delta_T) \frac{G}{G_n} \tag{25}$$

where $I_{PV,n}$ is the photovoltaic current at the standard test condition, $\delta T = T - T_n$ (in Kelvin) where T is the PV cell temperature and n denotes STC, G (watts per square meters) is the irradiation on the device surface, and G_n is the nominal irradiation. An assumption that $I_{sc,n} \approx I_{PV,n}$ is made because the series resistance of the single diode model is low and the parallel resistance is high. In summary, I_{PV} can be represented by equation 26, where all of the parameters can be obtained from data sheet values and from measurements.

$$I_{PV} = (I_{sc,n} + k_i \delta_T) \frac{G}{G_n} \tag{26}$$

For I_0, the diode saturation current and its dependence on the temperature can be expressed as equation 27:

$$I_0 = I_{0,n} (\frac{T}{T_n})^3 exp[\frac{qE_g}{Ak} (\frac{1}{T_n} - \frac{1}{T})] \tag{27}$$

where E_g is the bandgap energy of the semiconductor ($E_g = 1.12eV$ for the polycrystalline Si at 25°C) and $I_{0,n}$ is the nominal saturation current at the standard test conditions (STC), which could be expressed as follows:

$$I_{0,n} = \frac{I_{sc,n}}{exp(\frac{V_{oc,n}}{V_{t,n}}) - 1} \tag{28}$$

where $V_{t,n}$ is the thermal voltage at the standard test condition.

The PV panel model selected for this study is model KC200GT[3]. The geometric specifications of a single PV panel are 1425mm(56.2in)× 990mm(39.0in) which is comprised of 54 PV cells. The other detailed specifications available in the manufactures' datasheet to retrieve a single diode PV cell model are listed in table 5. Three important parameters (R_s,R_p and A) can be computed according to equations 24 based on required parameters in datasheet 5. The results are $R_s = 0.3625\Omega$, $R_p = 6928\Omega$ and $A = 1.0565$.

Table 5: KG200GT PV panel specifications

Electrical performance under standard test conditions	
Maximum Power (P_{mpp})	200W(+10% -5%)
Maximum Power Voltage (V_{mpp})	26.3V
Maximum Power Current (I_{mpp})	7.61A
Open Circuit Voltage (V_{oc})	32.9V
Short Circuit Current (I_{sc})	8.21A
Max System Voltage	600V
Temperature Coefficient of V_{oc}	-1.23×10^{-1} V/°C
Temperature Coefficient of I_{sc}	3.18×10^{-3} A/°C
Cells	
Number per Module	54
Physical specifications	
Length× Width× Depth	1425mm(56.2in)× 990mm(39.0in)× 36mm(1.4in)

The predicted electrical characteristics using the single diode PV cell model are shown in figure 6 and the experimental data is shown by circles. From comparisons of the results, the single diode model of PV cell model constructed according to the datasheet agrees well with the manufacturers' data.

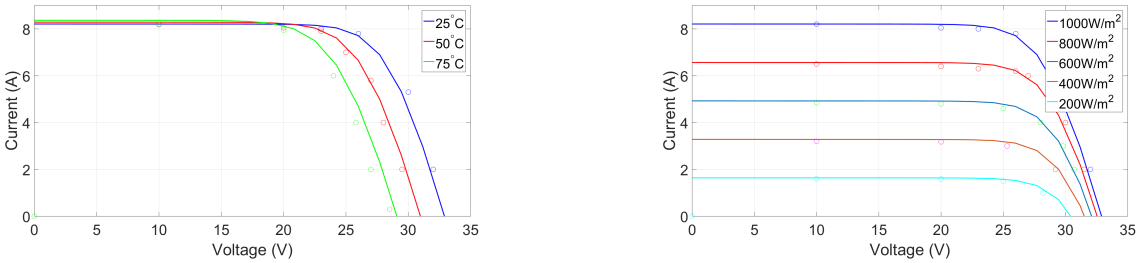

(a) Irradiance: AM1.5, 1000W/m^2

(b) Cell temperature: 25°C

Figure 6: I-V characteristics of PV module KC200GT prediction

4. Model Predictive control

The objective is to minimize the utility cost that consists of demand costs and TOU energy costs. Demand costs were determined based on 1-hour average power and TOU energy costs were charged based on 15-minute energy flows. The monthly utility bill was computed based on equation 29.

$$\sum_{i=0}^{N_e-1} E(i)P_{tb}^{15}(i)\Delta t + max(D(k)P_{tb}^{60}(k)|k \in \{0,\ldots,N_d-1\}) \tag{29}$$

where N_e is the number of 15-minute time intervals, E is the time of use energy rate, P_{tb}^{15} is the 15-minute average total building electrical power, Δt is the time step, D is the demand charge rate, P_{tb}^{60} is the 60-minute average total building electrical power and N_d is the number of hourly time intervals.

4.1. Ice storage and photovoltaic system model predictive control

In the MPC formulation, it is assumed that chilled water supply temperature to the load is fixed at 44°F. The objective of MPC is to determine the sequences of control inputs which are chiller modes M and chiller outlet setpoints $T_{CHe,SP}$ for the purpose of minimizing monthly utility bills. For the ice storage system, there are five modes which naturally results in a mixed integer nonlinear programming (MINLP) problem. Though MINLP can be used for analysis purposes, it is not preferred for MPC implementation. This is because there is a lack of freely available MINLP solvers and a MINLP-based MPC might be difficult to implement in an on-line solution since it may incur great computational effort such that it cannot be solved within the sampling time. In addition, it is hard to consider demand charges because of a limited prediction horizon which is imposed by prediction errors and computational issues.

In order to deal with the first issue, an approach that maps ice storage capacity into plant modes was developed that converts the original mixed integer nonlinear programming (MINLP) problem into a nonlinear programming (NP) problem solved by dynamic programming. For the second issue, a reformulation of the original optimization problem minimizes time-of-use energy cost treating the demand charge as an adjustable

constraint. If feasible solutions can not be found, a hard demand target is increased to the point where a feasible solution is found.

Using the ice storage cooling capacity (discharge rate) as an optimization variable and substituting the demand cost by variable z, the reformulated MPC problem with constraints is given as:

$$
\begin{aligned}
&\min_{z,u(0),\ldots,u(N-1)} \sum_{k=0}^{N-1} E(k)(P_{HVAC}(k)\Delta t - P_{solar}(k)\Delta t) + \omega \times z \\
&x_s(k+1) = x_s(k) - \frac{u(k)\Delta t}{C_s} \\
&0 \le Q_{CH}(k) \le Q_{CH,max}(T_{CH,i}(k), \dot{m}_{CH}(k), T_{OA}(k)) \\
&\begin{cases} u(k) \le Q_{IS,max,D}(T_{CH,e,SP}(k), \dot{m}_{CH}(k), x(k)) & if \quad (u(k) \ge 0) \\ -u(k) \le Q_{IS,max,C}(T_{CH,e,SP}(k), \dot{m}_{CH}(k), x(k)) & if \quad (u(k) < 0) \end{cases} \\
&Q_{CH}(k) = Q_{BL}(k) - u(k) \\
&T_{CHe,SP}(k) = \begin{cases} T_{CH,i}(k) - \frac{Q_{CH}(k)}{\dot{m}_{CH}(k) C_{p,w}} & if \quad (u(k) \ge 0) \\ 0 + \frac{u(k)}{\epsilon_C(\dot{m}_{CH}(k), x(k)) \dot{m}_{CH} C_{p,w}} & if \quad (u(k) < 0) \end{cases} \\
&T_{CH,i}(k) = T_{CHWS,SP}(k) + \frac{Q_{BL}(k)}{\dot{m}_{CH}(k) C_{p,w}} \\
&P_{HVAC}(k) = \begin{cases} 0 & if \quad (u(k) = 0, Q_{BL} = 0) \\ P_{CH}(Q_{CH}(k), T_{CH,e,SP}(k), T_{OA}(k)) + P_{pump}(\dot{m}_{CH}) & (otherwise) \end{cases} \\
&D(k)(P_{HVAC}(k) + P_{non,HVAC}(k) - P_{solar}(k)) \le z \quad (k \in \{0, \ldots, N-1\}) \\
&x_{s,l} \le x_s(k) \le x_{s,u}
\end{aligned}
\tag{30}
$$

where E(\$/kWh) is time-of-use energy cost and D(\$/kW) is demand charge. P_{HVAC} is the electric power associated with the HVAC system and $P_{non,HVAC}$ is the electric power excluding HVAC power. P_{solar} is the total PV panel generation rate, and Q_{BL} is the building cooling load. N is a look-ahead horizon which ideally should cover a billing period (one month). z is a demand limit which is also to be optimized and ω is a weighting number introduced to compensate for the reduced time period if N is less than the billing period. u is the control input to be optimized which is the ice storage cooling capacity (discharge rate) in the formulation. Variables required to be predicted are T_{OA} and Q_{BL}, which are assumed perfect predictions in this study. The variables of $T_{CH,i}, \dot{m}_{CH}, Q_{CH}$ and $T_{CHe,SP}$ are internal variables to be calculated for the chiller and ice-storage components.

The first constraint represents the ice storage dynamics using the concept of state of charge (SOC). The first inequality denotes the chiller capacity range at time step k. The second and third inequalities state capacity limits for the ice storage tank during discharging and charging processes at time step k. The equation for Q_{CH} specifies the cooling load left for the chiller after subtracting the ice storage capacity from the total building cooling load. The equation for $T_{CHe,SP}$ is switched depending on the ice-storage modes, where the first equation for the discharging process is simply an energy balance for the chiller and the second equation for the charging process is from the ϵ -NTU relation for the ice storage. The HVAC power includes chiller and pump power. If there is no building cooling load, and ice tanks are not charged, the HVAC power is set to 0. The second to last inequality denotes the demand limit constraint, and the last inequality specifies ice storage state of charge constraints ($x_{s,l} = 0$ and $x_{s,u} = 1$).

4.2. Battery and photovoltaic system model predictive control

For the battery system integrated with photovoltaics, the cooling plant only has "chiller-only" and "off" modes. For this system, the chiller cooling capacity should be sufficient to meet the peak building load. Similar to an ice storage system, the battery discharging (or charging) current rate is an optimization variable and the MPC problem was formulated as below:

$$
\begin{aligned}
&\min_{z,u(0),\ldots,u(N-1)} \sum_{k=0}^{N-1} E(k)(P_{HVAC}(k)\Delta t - P_{solar}(k)\Delta t - P_b(k)\Delta t) + \omega \times z \\
&x_b(k+1) = x_b(k) - \frac{u(k)\Delta t}{Q_{bat,I}} \\
&0 \le Q_{CH}(k) \le Q_{CH,max}(T_{CH,i}(k), \dot{m}_{CH}(k), T_{OA}(k), maxstage) \\
&Q_{CH}(k) = Q_{BL}(k) \\
&T_{CHe,SP}(k) = T_{CHWS,SP}(k) \\
&T_{CH,i}(k) = T_{CHWS,SP}(k) + \frac{Q_{BL}(k)}{\dot{m}_{CH}(k) C_{p,w}} \\
&P_{HVAC}(k) = \begin{cases} 0 \quad if \quad (Q_{BL} = 0) \\ P_{CH}(Q_{CH}(k), T_{CH,e,SP}(k), T_{OA}(k)) + P_{pump}(\dot{m}_{CH}) \quad (otherwise) \end{cases} \\
&D(k)(P_{HVAC}(k) + P_{non-HVAC}(k) - P_{solar}(k) - P_b(k)) \le z \quad (k \in \{0, \ldots, N-1\}) \\
&P_b(k) = F(u(k), x_b(k), \Delta t) \\
&x_{b,l} \le x_b(k) \le x_{b,u}
\end{aligned}
\tag{31}
$$

where u is the battery current (discharging is positive and charging is negative), P_b is the battery discharging (or charging) rate (kW) as a function of current (u), state of charge ($x_b(k)$) and time step (Δt), and $Q_{bat,I}$ is the battery capacity (Amp-hours). The battery's state of charge is constrained between 0.25 and 0.95 to avoid deep depletion and over-charging.

4.3. Demand limit reset strategy

The two proceeding MPC formulations can be represented in a condensed way:

$$
\begin{aligned}
&\min_{z,u(0),\ldots,u(N-1)\in U} \quad \sum_{k=0}^{N-1} E(k) P_t(k) \Delta t + \omega \times z \\
&\text{s.t.} \quad D(k) \times (P_t(k) + P_{non,HVAC}(k)) \le z \quad \forall k \in \{0, \ldots, N-1\}
\end{aligned}
\tag{32}
$$

where P_t for an ice storage system is $P_{HVAC}(k) - P_{solar}(k)$ and for a battery system is $P_{HVAC}(k) - P_{solar}(k) - P_b(k)$. U represents a feasible set of control variables imposed by dynamics, equality and inequality constraints. In the MPC, time-of-use energy costs are assumed to be charged based on 1-hour average power, consistent with the demand costs. Ideally, N should cover a billing period which is one month. However, it is not practical to consider an entire monthly time horizon because of computational requirements and prediction uncertainties of disturbances such as outdoor temperature and occupancy. A typical MPC strategy to consider a demand charge in the literature is to set N to a reduced prediction horizon, e.g., one day in this study. The MPC formulation expressed in 32 can be simplified further into 33 which only solves the time-of-use energy cost minimization problem with a demand limit constraint in order to obtain a suboptimal solution with a reduced computation time.

$$\min_{u(0),\ldots,u(N-1)\in U} \quad \sum_{k=0}^{N-1} E(k)P_t(k)\Delta t \tag{33}$$
$$\text{s.t.} \quad D(k) \times (P_t(k) + P_{non,HVAC}(k)) \leq \hat{z}_m^* \quad \forall k \in \{0,\ldots,N-1\}$$

The final MPC and demand limit reset algorithm proposed is shown below.

input : meteorological data, utility rate

1 For the first decision making time of a billing period, initialize
$\hat{z}_M^* = \hat{z}_{M,0}^* = \max\{D(k)P_{non,HVAC}(k)|k \in \{0,\ldots,N-1\}\}$
2 **while** *simulation* **do**
3 **if** *at decision making time* **then**
4 Solve the energy cost optimization problem 33 by dynamic programming.;
5 **if** *there exists a feasible solution* **then**
6 maintain $\hat{z}_M^*$ to the next decision making time and implement the optimal control input sequence;
7 **else**
8 increase $\hat{z}_M^*$ by 5% of $\hat{z}_{M,0}^*$ and return to line 3;
9 **end**
10 **else**
11 implement the optimal control sequence determined at the last decision making time
12 **end**
13 **end**

Algorithm 1: MPC and demand limit reset algorithm

The MPC algorithm was implemented through dynamic programming. The following figures illustrate system responses determined by the MPC controller for both the ice storage and battery systems. It should be mentioned that all the components were not optimally sized. The goal here is to compare optimal control system response differences for systems with ice storage or batteries. Figure 7(a) illustrates the responses for a 75-ton central cooling plant coupled with a 330 ton-hour ice storage and a 40 kW PV array under the proposed MPC controller. The black dash line denotes the scaled on-peak, partial-peak and off peak electricity cost rates. For August 2nd, all of the HVAC load was shifted into the off-peak period. However there was a power peak for power purchased from the grid. In this case, this is the difference between non-HVAC load and PV generation rate. Even though in commercial buildings non-HVAC load is pretty flat and stable, after integration with renewable energy resources, e.g., PV, there could still be power peaks for purchasing electricity. Figure 7(b) shows the responses of a 75-ton central cooling plant coupled with a 0.5 C-rate 385 kWh lithium-ion battery bank and a 40 kW PV array under MPC. The battery size was determined to be similar to the ice storage size considering the conversion from cooling to electricity requirements using a typical COP. It could be observed that batteries respond to the total building load peak by releasing more energy such that the net power purchased from the utility grid doesn't have a power spike. This is due to the flexibility of batteries that can shift both HVAC and non-HVAC loads as compared to a case of the ice storage system. Hence, batteries are more effective for shaving peak power when a system is coupled with PV.

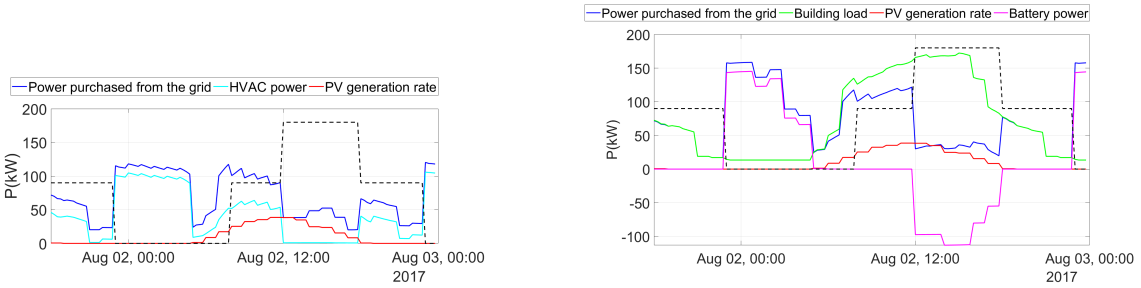

(a) On-site PV coupled with Ice Storage

(b) On-Site PV coupled with Battery Storage

Figure 7: Responses of system under MPC controller

5. Optimal system component sizing and system comparisons

An answer to the question of which system between "chiller + PV + ice storage" and "chiller + PV + battery" is economically better depends on a selection of each component size. To ensure fair comparisons, we optimized sizes of chiller, PV and storage for each system (by minimizing the life cycle cost, LCC), and compared the minimal LCCs for the two systems.

The first optimal-sizing process requires a two-level optimization where the higher level optimizes the component sizes, and the lower level optimizes the operation for given sizes. This is because the former determines the capital cost while the latter determines the operation cost. The co-optimization process is computationally expensive and numerically challenging especially for the ice-storage system. To tackle this problem, in this section, we also present a numerical approach which sequentially sizes the components for the ice-storage system.

5.1. Optimal sizing for chiller and ice storage system without PV

5.1.1. Search region for chiller and storage size combinations

In order to evaluate life cycle costs for different size combinations of chiller and ice storage, the first step is to determine the feasible search region. Figure 8 shows the search region, i.e., the shaded region, which was considered in this research. The horizontal and vertical axes denote the chiller capacity and ice storage capacity respectively. The point "A" is partial storage sizing that minimizes the chiller and ice storage sizes, and the associated installed costs when storage is utilized. Point "B" is a conventional system without storage that only uses the chiller to provide cooling throughout the day. Point "C" is a full storage system with maximum ice storage and chiller capacity. The bottom boundary of the search region is the minimum ice storage capacity as a function of chiller capacity such that the system could meet the design day cooling load. The minimum storage capacity decreases with increasing chiller capacity since with a greater chiller capacity the remaining cooling load to be met by ice storage is less. The upper boundary contains an inclined line and a horizontal line. The inclined line represents the maximum ice storage capacity that a given sized chiller could fully charge during unoccupied hours on the design day. The slope is upward since a greater chiller capacity can produce more ice. The horizontal line specifies the minimum ice storage capacity required to meet the on-peak building load by itself, beyond which the extra capacity is useless incurring some unnecessary initial costs. The intersection of these two lines at point C is the full storage design point where the ice storage capacity is sufficient to meet the on-peak building load and the chiller capacity is the

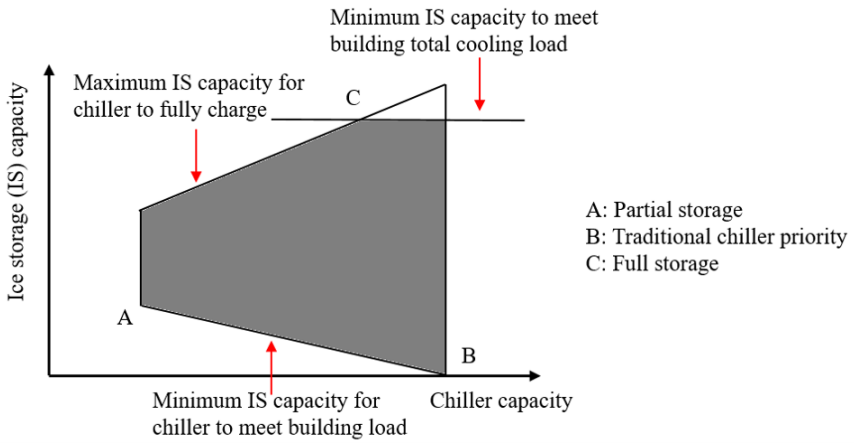

Figure 8: Schematic of the search region

minimum necessary to fully charge it during the unoccupied period. The left and right boundaries are both determined by the chiller capacity which specify the minimum and maximum chiller capacity, respectively.

Conventionally, points "A", "B" or "C" are used depending on cost considerations, utility rates, and control strategies. A rule of thumb is that the partial storage sizing has much better economics than the full storage and traditional HVAC system in terms of the life cycle cost when appropriate utility incentives are in place. The partial storage system can spread out building loads evenly throughout the day, and minimizes chiller and ice storage sizes. The full storage system has the highest investment cost which typically leads to greater life cycle cost than partial storage even though the operating costs are lower.

An intriguing question that naturally comes from the figure 8 is whether the partial storage system is the point having the minimum life cycle cost among the search region or not.

5.1.2. Life cycle cost graph

An optimal sizing strategy for the chiller and ice storage in terms of life cycle costs should employ optimal control for all possible size combinations within the search region (figure 8). In order to generate a life cycle cost graph over the search region, it is necessary to sample many points among the search region where each point is an annual simulation. The life cycle cost depends on both initial costs of components and operating costs, which depend on building type, climate zone and utility rates to be considered. Operating costs were calculated by optimizing the operation using the MPC explained in the previous section. This study addresses optimal chiller and storage sizes for the case study. Utility rates, the life-cycle financial performance metric and system component installed costs are described in table 2-4. Life cycle cost graphs for three typical California utility rate plans for commercial buildings are shown in figure 9, 10 and 11.

From the life cycle cost graphs and contours for the three utility rate plans, the minimum life cycle cost is near the minimum chiller and ice storage size. In addition, the variation in life-cycle costs near this point is pretty small. The life cycle cost magnitude and variation near the full storage and conventional HVAC systems are much higher than the region around the partial storage point. For simplicity, the optimal chiller and ice storage sizes for these three utility rate plans can be selected as a partial storage system.

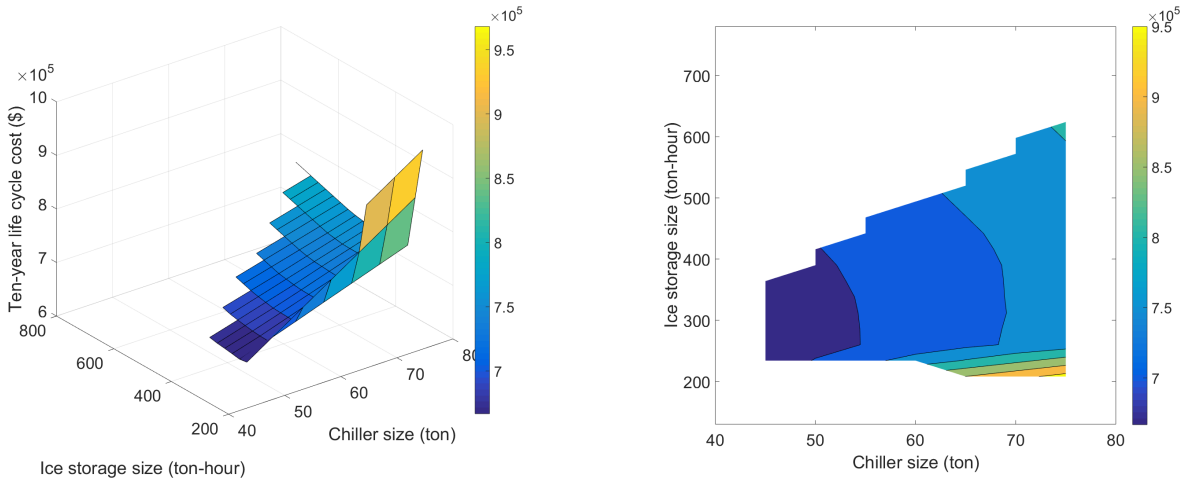

(a) Life cycle cost graph

(b) Life cycle cost contour

Figure 9: Utility rate A10 life cycle cost for cooling plant with IS (w/o PV) under an optimal operation

5.2. Optimal sizing for chiller and ice storage system with PV

Two sizing strategies for PV combined with a central cooling system coupled with ice storage were considered. The first one involves directly searching for the optimal PV size in terms of life cycle cost with the proposed MPC algorithm implemented for a prescribed partial storage system. The second method attempts to reduce the computational effort by decoupling the control and sizing processes. This sequential optimal sizing scheme is validated using the direct search method.

5.2.1. Direct Search

The optimal sizes of chiller and ice storage are assumed to be the partial storage solution since the cost sensitivity around this region is small. With this prescribed central cooling plant size, the simplest method to size a PV system is to perform annual simulations with the proposed MPC algorithm for different PV sizes and find the size that minimizes the life cycle cost. This method is termed direct search.

5.2.2. Sequential Optimization

The direct search method, though precise, is time-consuming. In order to reduce computational effort, the control and sizing can be decoupled into two phases. In the first phase, annual simulations of the partial storage system along with MPC are performed. An electrical load profile from this first phase is then used as an input to a second phase for sizing the PV system. The second phase determines the optimal PV size according to the following optimization problem 34.

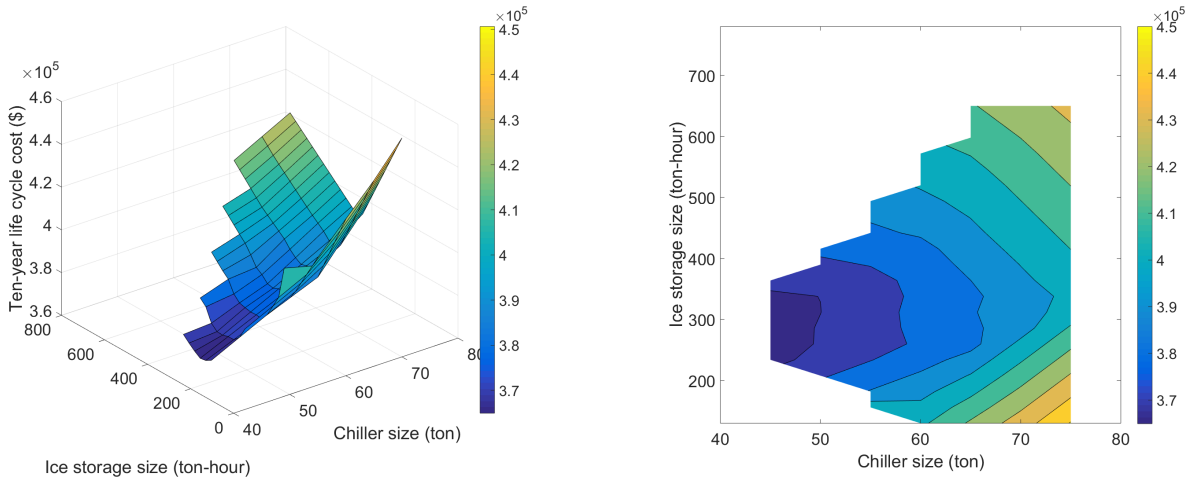

(a) Life cycle cost graph

(b) Life cycle cost contour

Figure 10: Utility rate GS-2B life cycle cost for cooling plant with IS (w/o PV) under an optimal operation

$$
\begin{aligned}
\min_{n \in Z} \quad & C^i_{PV} n + P_w \Big(\sum_{i=1}^{N_y} E(i) P_g(i) \Delta t + \sum_{j=1}^{N_m} \max_{k \in \mathcal{I}_j} (D(k) P_g(k), 0) + C^m_{PV} n\Big) \\
\text{s.t.} \quad & P_g(i) = P_l(i) - P_s(i) \\
& \sum_{i=1}^{N_y} E(i) P_g(i) \Delta t \geq 0 \\
& P_s(i) = n P_{si}(i) \\
& n \geq 0
\end{aligned} \tag{34}
$$

where n is the number of PV panels (Model KC200GT for this study), C^i_{PV} is the installed cost per PV panel (1.88 \$/W installed cost for this study), C^m_{PV} is the maintenance fee per PV panel (assuming 18 \$/kW per year for maintenance), N_y is the total number of hourly time intervals in one year, N_m is the number of months, e.g., 12 for a year, $\mathcal{I}_j$ denotes the subset of i that belongs to j, i.e., all indices of hourly time intervals that belong to jth month of a year, P_g is the net hourly average power purchased from the grid (kW), P_l is the hourly average building electricity load (kW), P_s is the total hourly average PV power generation rate (kW), P_{si} is the single PV panel power (kW) and P_w is the present worth factor for ten years associated with currency inflation and discount.

In optimization problem 34, P_l, P_{si}, E, D and P_w are all inputs. The first constraint is an energy balance on power for the building. The second constraint is based on the net energy metering policy that has an annual true-up such that the annual cumulative energy cost should be greater than 0 which gives an upper bound for PV capacity. The third equation calculates the total hourly average PV power generation rate of n PV panels. The last constraint simply denotes a lower bound for the PV panel number.

In the optimization problem, P_l is unknown for a system coupled with ice storage for the reason that ice storage can reshape the building electrical load. Different control decisions provide different building load

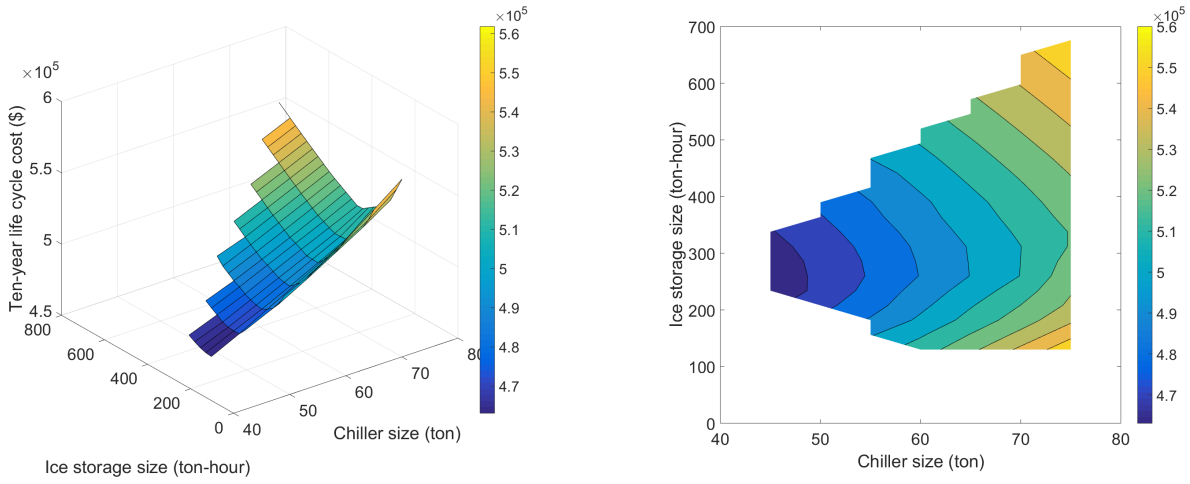

(a) Life cycle cost graph

(b) Life cycle cost contour

Figure 11: Utility rate GS-R life cycle cost for cooling plant with IS (w/o PV) under an optimal operation

profiles because of load shifting. Ideally, the control and sizing should be processed simultaneously. The sequential optimization method eliminates this coupling and runs a single annual simulation for a partial storage system with MPC but without PV. The building load profile from this simulation is then used as an input to the optimization problem 34 as P_l. Due to the efficiency and robustness of convex optimization, the optimal PV panel number n could be computed rapidly in a convex programming solver.

5.2.3. Optimal PV sizing validation

A summary of the optimal PV panel numbers for utility rate plan A10, GS-2B and GS-R are listed in table 6. The optimal PV sizes determined by the direct search method serve as the baseline for evaluating the sequential optimization.

Table 6: Optimal PV panel number validation

Utility rate plan	Optimal PV panel number (Coupling control and sizing)	Optimal PV panel number (Decoupling control and sizing)
A10	900	901
GS-2B	0	0
GS-R	795	795

For utility rate A10, the optimal PV panel number computed by sequential optimization is 901, which is almost the same as the direct search optimal number of 900. For both approaches, the optimal PV panel numbers result in an annual energy cost of 0. Thus, the TOU energy rate for utility rate A10 is high enough so that the best decision is to use as much PV panel as possible. The maximum PV panel number is determined by the second constraint in optimization problem 34. The optimal PV panel numbers for GS-2B computed by the two methods are both exactly 0 for the reason that GS-2B has a relatively low TOU energy cost rate such that the pay back period for installation of PV is longer than ten years. The utility rate

GS-R has a much higher TOU energy cost rate than utility rate GS-2B such that the optimal size of PV is again to install as much as possible leading to an annual energy cost of 0. For all three cases, the sequential optimization approach gives essentially the same result as the direct search method.

5.3. Optimal sizing for chiller and battery with PV

Optimal sizing for PV with batteries in terms of life cycle costs should be carried out in combination with optimal control. In the design stage, both demand and energy costs can be minimized to obtain a theoretical optimal solution using perfect knowledge of ambient conditions and building loads. The optimization problem for sizing battery and photovoltaics is formulated as follows in 35:

The optimization variables are n, C_b and $P_b(i)$ which are the number of PV panels, battery energy storage capacity (kWh) and hourly battery discharging and charging rates (kW). In the objective function, C^i_{ba} is the battery installed cost per unit of energy storage capacity (\$/kWh) and C^m_{ba} is the battery maintenance cost(\$/kWh per year). C_r is the battery C-rate which in this study is 0.5. P_w is the net present factor for a ten-year analysis. The first constraint is the building electrical energy balance with a definition that battery discharging is positive and charging is negative. The initial state of charge, i.e., $x_{b,ini}$, is taken to be 0.25. The third constraint represents the battery dynamics. For the purpose of simplicity in the optimal sizing phase, the battery power rate lower and upper bounds are only determined by its C-rate, i.e., 0.5 in this study. In addition, battery state of charge is restricted between 0.25 and 0.95 to prevent over depletion and charge.

Figure 12 shows optimal system life cycle cost and optimal PV panel number for utility rate A10 determined by varying battery capacities. Subfigure 12(a) shows that with the current installed costs (454 \$/kWh), the optimal installed battery energy storage capacity is 90 kWh which leads to a 2.5 % life-cycle cost savings. Subfigure 12(b) shows variation of optimal PV panel number with battery capacity. The scale is quite small and the optimal PV size has a small dependence on battery capacity.

$$
\begin{aligned}
\min_{n\in Z, C_b\in R, P_b(i)\in R} \quad & C^i_{PV}n + C^i_{ba}C_b + P_w\Big(\sum_{i=1}^{N_y} E(i)P_g(i)\Delta t + \sum_{j=1}^{N_m}\max_{k\in\mathcal{I}_j}(D(k)P_g(k),0)\Big) + C^m_{PV}n + C^m_{ba}C_b\Big) \\
\text{s.t.} \quad & P_g(i) = P_l(i) - P_b(i) - P_s(i) \\
& x_b(0) = x_{b,ini} \\
& x_b(i+1) = x_b(i) - \Delta t\frac{P_b(i)}{C_b} \\
& -C_rC_b \le P_b(i) \le C_rC_b \\
& x_{b,l} \le x_b(i) \le x_{b,u} \\
& \sum_{i=1}^{N_y} E(i)P_g(i)\Delta t \ge 0 \\
& P_s(i) = nP_{si}(i) \\
& n \ge 0
\end{aligned}
\tag{35}
$$

5.3.1. Sensitivity of optimal battery size to installed costs

Even though the current installed cost for lithium-ion batteries is not significantly favorable for integration, it is expected that the price will drop in the future. Figure 13 shows ten-year life cycle cost variation

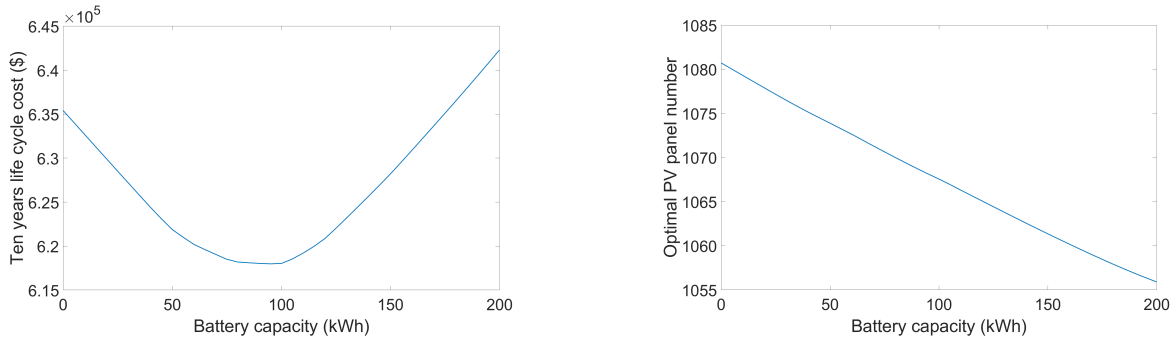

(a) Ten years life cycle cost

(b) Optimal PV panel number

Figure 12: Variation of system optimal life cycle cost and PV size versus battery capacity for utility rate plan A10

versus battery capacities for three installed costs of batteries of 454 $/kWh, 300 $/kWh and 100 $/kWh for utility rate plan A10. Solid lines and dashed lines represent ten-year life cycle costs and relative life cycle cost savings compared with the baseline that doesn't incorporate batteries and PV arrays, respectively. For the two lower battery costs, there is an optimal battery capacity of 110 kWh for 300 $/kWh with a 5.2 % life-cycle cost savings, and 265 kWh for 100 $/kWh with a 10.4 % life-cycle cost savings. Both cases illustrate a promising cost saving potential when the initial cost of battery drops with technology development in the future.

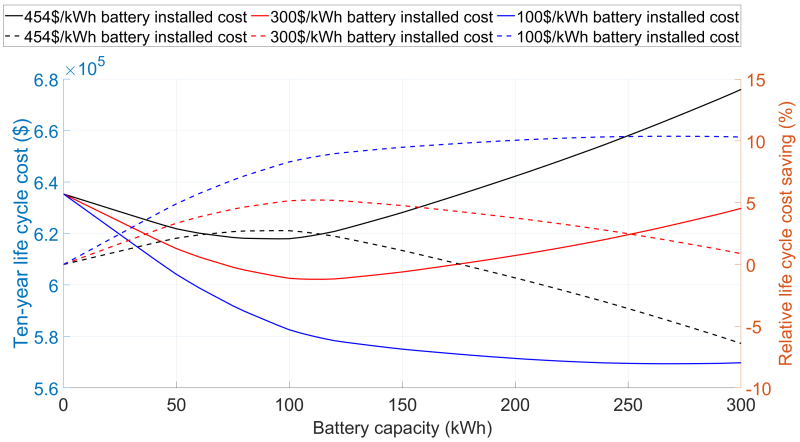

Figure 13: Variation of system optimal life cycle cost versus battery capacity under different battery installed costs for utility rate plan A10

6. Economic comparison between ice storage or batteries for a chiller plant with PV

6.1. System component optimal size selection

Table 7 summarizes the system component optimal sizing results for the case study in terms of the life cycle cost.

For the central cooling system coupled with ice storage, the optimal ice storage and PV sizes were determined in two stages. The ice storage optimal size was taken to be a partial storage point since the life cycle cost sensitivities in this region are quite low for all three utility rate plans. The PV size was then computed from the optimization problem 34. Since utility rate A10 and GS-R have high TOU-energy rates, the optimal PV size is the maximum PV size. On the contrary, utility rate GS-2B has a much lower TOU-energy rate such that not integrating PV is optimal in view of optimal life cycle cost.

For the central cooling system coupled with lithium-ion batteries, the chiller size is determined by the design day building cooling load and a 75-ton chiller was selected for all three cases. The optimal battery storage capacity and PV sizes were determined by solving the optimization problem shown in equation 35. Since utility rate A10 has an any-time demand costs, charging batteries is penalized during the off-peak hours and a 214 kW PV array should compensate for this accordingly. Utility rate plans GS-2B and GS-R have no off-peak demand costs such that fully utilizing batteries to perform load shifting is encouraged when battery installed costs are favorable. As a result, the optimal battery capacities for these two utility rate plans are maximized and the PV sizes are 0 kW.

Table 7: System component optimal size selection

Central cooling system coupled with PV and ice storage			
	A10	GS-2B	GS-R
Chiller	45 ton	45 ton	45 ton
Ice storage	312 ton-hour	312 ton-hour	312 ton-hour
Photovoltaics	180 kW	0 kW	159 kW
Central cooling system coupled with PV and batteries			
	A10	GS-2B	GS-R
Chiller	75 ton	75 ton	75 ton
Battery	90 kWh	290 kWh	580 kWh
Photovoltaics	214 kW	0 kW	0 kW

6.2. Optimal life cycle cost

Life-cycle cost results for the different systems are summarized in figure 14. The baseline is a conventional HVAC system with a 75-ton chiller to meet the building cooling load and no PV or ice storage. The second bar in the figure is the life cycle cost for a central cooling system coupled with ice storage. The last two represent the optimal life cycle cost results for a central cooling system integrated with solar energy and either coupled with ice storage or battery storage.

For utility rate plan A10, the system coupled with solar energy and thermal storage significantly reduces life cycle costs giving up to 34 % savings. Since the optimal PV size is 0 for utility rate plan GS-2B, the life cycle costs of the ice storage system either coupled with or without PV are identical with 25 % savings. The third case shows that the system coupled with batteries and PV provides the most life cycle savings of 45 % under utility rate GS-R.

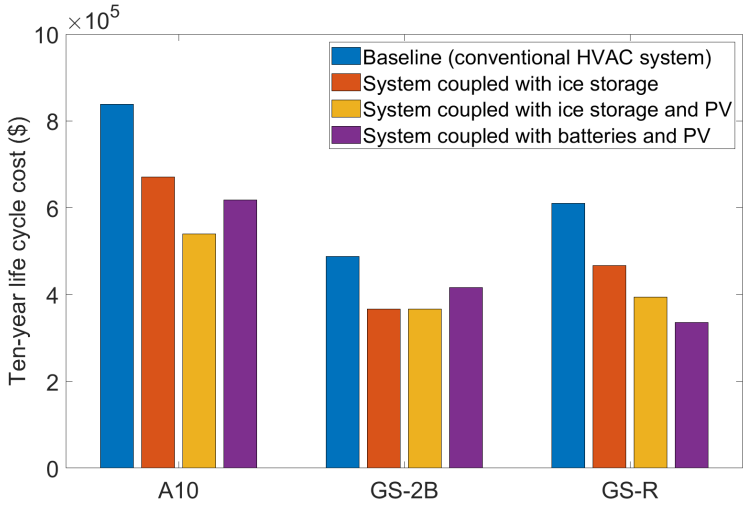

Figure 14: Summary of life cycle costs

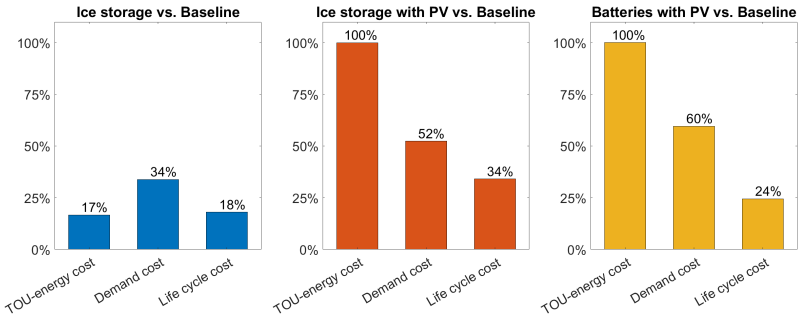

Figure 15: Relative cost savings for utility rate plan A10

Figures 15, 16 and 17 show the relative annual TOU-energy cost, demand cost, and life cycle cost savings in a comparison with the baseline for the three utility rate plans. For utility rate Plan A10, the system coupled with ice storage and PV gives the maximum life cycle cost savings of 34 % and 100 % TOU-energy cost savings as the system coupled with batteries and PV. However, the latter has a higher demand cost saving of 60 %, which is the result of the flexibility of batteries that can shave the non-HVAC load peak. Since the any time demand charge scheme penalizes further charging batteries during off-peak hours, the benefits come from batteries are limited. For utility rate plan GS-2B, the TOU-energy costs are low so that the optimization results in no solar PV for the ice storage system, and subfigures 1 and 2 of figure 16 are identical. The system coupled with batteries and PV provides higher savings of TOU-energy cost and demand cost, but the life cycle cost savings are less due to high installed costs. For the utility rate plan GS-R, the system coupled with batteries and PV has the higher life cycle cost savings of 45 % and TOU-energy cost savings of 100 % since batteries can be fully taken advantage of without demand charge limitations.

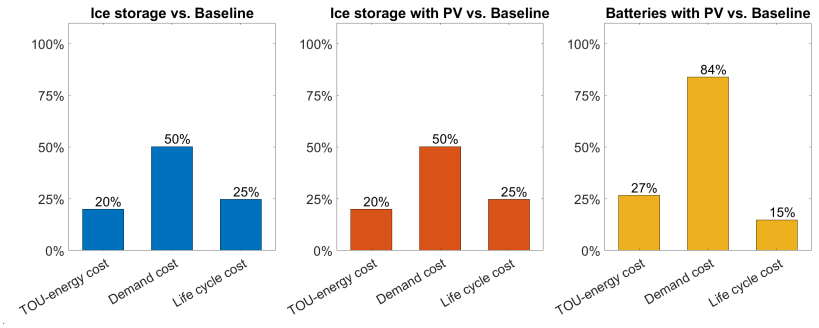

Figure 16: Relative cost savings for utility rate plan GS-2B

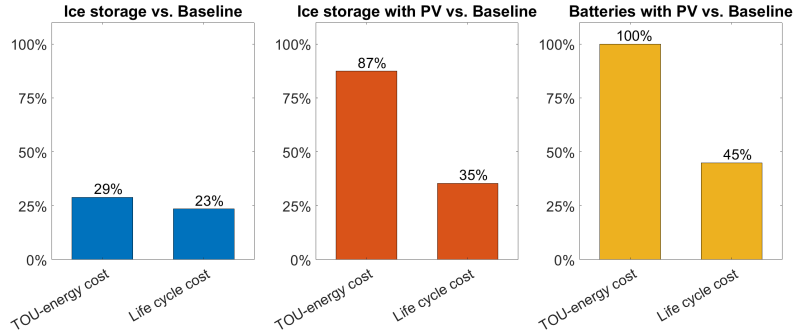

Figure 17: Relative cost savings for utility rate plan GS-R

7. Summary and Conclusions

This research focused on evaluation of the economic performance of a central cooling system with a photovoltaic array coupled with either thermal ice or battery storage. A case study for a medium size commercial building located in Riverside, California was performed. Three different representative utility rate plans were considered: TOU energy costs with an any time demand charge (A10), TOU energy costs with TOU demand charges (GS-2B), and only TOU energy costs (GS-R). A net energy metering policy was assumed throughout the case study which allows customers to sell back their self-generated power into the grid at the same retail price.

A simulation testbed was developed using empirical and semi-empirical modeling approaches that includes an air-cooled chiller, ice storage tanks, pumps, building loads, batteries and PV array models. The chiller model determines maximum cooling capacity which serves as one of the constraints in an MPC problem and electrical power associated with a certain building load and operating conditions. A lumped ice storage model was implemented based on the concept of state of charge (SOC) and heat transfer effectiveness that accounts for energy efficiency penalties during charging and discharging processes. A detailed lithium-ion battery model from Matlab Simulink was used to obtain a simplified linear interpolation input-output model. A PV model was implemented based on a single diode with five unknown parameters that were obtained from a manufacturer's data sheet.

A fast model predictive control algorithm was developed that could accomplish an annual simulation within a relatively short time. The near-optimal solution was facilitated by converting the original mixed-

integer nonlinear programming (MINLP) problem into a nonlinear programming (NP) problem and by changing the original combined energy cost and demand charge minimization problem into only minimizing short-term energy costs with a demand limit constraint. This NP problem was solved by backward dynamic programming in order to obtain a global optimal solution.

For a fair economic comparison, optimal system component sizing approaches were developed for each system. The system coupled with ice storage was sized by separating the central cooling plant and PV sizing into two sequential steps. Firstly, optimal life cycle cost graphs were generated by varying chiller and ice storage sizes for three utility rate plans. For all three plans, it could be visualized that the minimum life cycle cost point is near the minimum chiller and ice storage sizes, which is the partial storage point. In addition, the sensitivity of life cycle cost to the sizing near the partial storage system point is pretty low such that the optimal chiller and ice storage size could be simply selected as partial storage. Next, a simplified method was developed to optimally size the PV capacity for the prescribed partial storage system through decoupling control and sizing into two phases. This sequential optimization approach was validated through comparison with a baseline approach that coupled control and sizing. The results showed the simplified approach works very well with a small error shown in table 6. For the case of the system coupled with batteries, an optimization problem was developed that couples control and sizing.

The best system combination depends on the utility rate plan structure. The system coupled with ice storage and PV, the system coupled with ice storage, and the system coupled with batteries and PV are the best for utility rate plan A10, GS-2B, and GS-R, respectively, for the current installed cost estimates in table 4. A sensitivity analysis of lithium-ion battery installed costs showed that with declining costs of batteries it is expected that it will be increasingly economically beneficial and feasible to include battery storage in commercial buildings in the future.

8. NOMENCLATURE

$C_{p,w}$: specific heat of water/glycol mixture fluid

C^i_{PV} : installed cost per PV panel

C^m_{PV} : annual maintenance fee per PV panel

C^i_{ba} : battery installed cost per unit of energy storage capacity

C^m_{ba} : battery annual maintenance cost per unit of energy storage capacity

C_s : total ice storage capacity

C_b : battery energy storage capacity

C_r : battery C-rate

CWL : building cooling load

D : demand charge rate

DP : pressure differentials

E : time of use energy rate

I : battery charging and discharging current

M : plant modes

$\dot{m}_s$: mass flow rate passing two ice storage tanks

$\dot{m}_{0,s}$: mass flow rate passing two ice storage tanks at test conditions

$\dot{m}_{CH}$: mass flow rate passing chiller

$\dot{m}_{CHWR}$: mass flow rate from buildings

n : number of PV panels

N_e : number of 15-minute time intervals

N_d : number of hourly time intervals

N_y : number of hourly time intervals in one year

N_m : number of months

N_s : number of ice tanks

P_{tb}^{15} : 15-minute average total building electrical load

P_{tb}^{60} : 60-minute average total building electrical load

P_b : battery charging and discharging power

P_{pump} : pump power

P_{CH} : chiller plant power

P_g : net hourly average power purchased from grid

P_l : hourly average building electricity load

P_g : net hourly average power purchased from grid

P_s : total hourly average PV power generation rate

P_{si} : single PV panel power

P_w : present worth factor

Q_{CH} : chiller cooling capacity

Q_{CHL} : chiller cooling load to meet $T_{CHe,SP}$

$Q_{CH,max}$: maximum chiller cooling capacity

Q_{BL} : building cooling load

Q_{ISL} : ice storage cooling load to meet $T_{CHWS,SP}$

$Q_{IS,max}$: maximum ice storage capacity

$Q_{IS,CR}$: ice storage charing rate

Q_{IS} : ice storage charging and discharging rates

$Q_{bat,I}$: battery current capacity

Q_{bat} : battery energy capacity

SC_{PV} : Present Value of system costs

T_{OA} : outdoor dry bulb temperature

$T_{CHe,SP}$: chiller exit temperature setpoint

$T_{CHWS,SP}$: primary chilled water supply temperature setpoint

$T_{CH,i}$: chiller inlet temperature

$T_{CH,e}$: chiller exit temperature

$T_{s,i}$: ice storage inlet temperature

$T_{s,e}$: ice storage outlet temperature

T_{CHWR} : return water temperature from building

T_{fr} : freezing point temperature

u_{IS} : specific internal energy of the water and ice mixture

u_f : internal energy of saturated liquid water

u_{sf} : latent heat of fusion for ice

x_s : ice storage state of charge

x_b : battery state of charge

Δt : dicretized time step

$\epsilon_{0,C}$: ice storage charging heat transfer effectiveness for the test flow rate

$\epsilon_{0,D}$: ice storage discharging heat transfer effectiveness for the test flow rate

ϵ_C : ice storage charging heat transfer effectiveness

ϵ_D : ice storage discharging heat transfer effectiveness

η_{pump} : pump efficiency

η_{motor} : motor efficiency

$\eta_{inveter}$: inverter efficiency

9. REFERENCES

References

[1] Decision adopting successor to net energy metering tariff, California Public Utilities Commission, 2016.

[2] D. Sera, R. Teodorescu, P. Rodriguez, Pv panel model based on datasheet values, in: 2007 IEEE international symposium on industrial electronics, IEEE, 2007, pp. 2392–2396.

[3] M. G. Villalva, J. R. Gazoli, E. Ruppert Filho, Comprehensive approach to modeling and simulation of photovoltaic arrays, IEEE Transactions on power electronics 24 (5) (2009) 1198–1208.

[4] J. E. Braun, A comparison of chiller-priority, storage-priority, and optimal control of an ice-storage system, ASHRAE Trasaction 98 (1992) 893–902.

[5] K. H. Drees, J. E. Braun, Development and evaluation of a rule-based control strategy for ice storage systems, HVAC&R Research 2 (4) (1996) 312–334.

[6] J. Drgoňa, J. Arroyo, I. C. Figueroa, D. Blum, K. Arendt, D. Kim, E. P. Ollé, J. Oravec, M. Wetter, D. L. Vrabie, et al., All you need to know about model predictive control for buildings, Annual Reviews in Control 50 (2020) 190–232.

[7] J. Candanedo, V. Dehkordi, M. Stylianou, Model-based predictive control of an ice storage device in a building cooling system, Applied Energy 111 (2013) 1032–1045.

[8] Y. Ma, A. Kelman, A. Daly, F. Borrelli, Predictive control for energy efficient buildings with thermal storage: Modeling, stimulation, and experiments, IEEE control systems magazine 32 (1) (2012) 44–64.

[9] S. J. Cox, D. Kim, H. Cho, P. Mago, Real time optimal control of district cooling system with thermal energy storage using neural networks, Applied energy 238 (2019) 466–480.

[10] K. J. Kircher, K. M. Zhang, Model predictive control of thermal storage for demand response, in: 2015 American Control Conference (ACC), IEEE, 2015, pp. 956–961.

[11] R. Tang, S. Wang, Model predictive control for thermal energy storage and thermal comfort optimization of building demand response in smart grids, Applied Energy 242 (2019) 873–882.

[12] J. Braun, et al., Supervisory control strategies and optimization, ASHRAE Applications Handbook (2015) 64.

[13] Y. Lu, S. Wang, Y. Sun, C. Yan, Optimal scheduling of buildings with energy generation and thermal energy storage under dynamic electricity pricing using mixed-integer nonlinear programming, Applied Energy 147 (2015) 49–58.

[14] J. Vetterli, M. Benz, Cost-optimal design of an ice-storage cooling system using mixed-integer linear programming techniques under various electricity tariff schemes, Energy and buildings 49 (2012) 226–234.

[15] J. West, J. E. Braun, Modeling partial charging and discharging of area-constrained ice storage tanks, HVAC&R Research 5 (3) (1999) 209–228.

[16] T. R. Ran Fu, R. Margolis, 2018 U.S. utility-scale photovoltaics-plus-energy storage system costs benchmark, National renewable energy laboratory, 2018.

[17] D. F. Ran Fu, R. Margolis, U.S. solar photovoltaic system cost benchmark: Q1 2018, National renewable energy laboratory, 2018.

[18] D. susan schoenug, Ph, Energy storage systems cost update, Sandia national laboratories, 2011.

[19] X. Jin, A. Vora, V. Hoshing, T. Saha, G. Shaver, R. E. García, O. Wasynczuk, S. Varigonda, Physically-based reduced-order capacity loss model for graphite anodes in li-ion battery cells, Journal of Power Sources 342 (2017) 750–761.

[20] A. Nottrott, J. Kleissl, B. Washom, Energy dispatch schedule optimization and cost benefit analysis for grid-connected, photovoltaic-battery storage systems, Renewable Energy 55 (2013) 230–240.

[21] I. Ranaweera, O.-M. Midtgård, Optimization of operational cost for a grid-supporting pv system with battery storage, Renewable Energy 88 (2016) 262–272.

[22] J. Cai, X. Jin, H. Zhang, Economic model-based control of sustainable buildings with photovoltaic (pv) and battery systems considering battery degradation costs, in: 2018 Annual American Control Conference (ACC), IEEE, 2018, pp. 5406–5411.

[23] J. Li, M. A. Danzer, Optimal charge control strategies for stationary photovoltaic battery systems, Journal of Power Sources 258 (2014) 365–373.

[24] C. R. Touretzky, M. Baldea, Integrating scheduling and control for economic mpc of buildings with energy storage, Journal of Process Control 24 (8) (2014) 1292–1300.

[25] X. Wang, M. Dennis, Influencing factors on the energy saving performance of battery storage and phase change cold storage in a pv cooling system, Energy and Buildings 107 (2015) 84–92.

[26] M. Saffari, A. de Gracia, C. Fernández, M. Belusko, D. Boer, L. F. Cabeza, Optimized demand side management (dsm) of peak electricity demand by coupling low temperature thermal energy storage (tes) and solar pv, Applied energy 211 (2018) 604–616.

[27] B. Zhao, Z. Zhao, M. Huang, X. Zhang, Y. Li, R. Wang, Model predictive control of solar pv-powered ice-storage air-conditioning system considering forecast uncertainties, IEEE Transactions on Sustainable Energy 12 (3) (2021) 1672–1683.

[28] B. Pandey, R. Banerjee, Feasibility analysis of pv-battery and pv-tes for cooling application in buildings, in: Urban Science and Engineering, Springer, 2021, pp. 313–324.

[29] C. Luerssen, O. Gandhi, T. Reindl, C. Sekhar, D. Cheong, Life cycle cost analysis (lcca) of pv-powered cooling systems with thermal energy and battery storage for off-grid applications, Applied Energy 273 (2020) 115145.

[30] T. Stuhlenmiller, R. Koenigsdorff, Optimum thermal storage sizing in building services engineering as a contribution to virtual power plants, Journal of Building Performance Simulation 3 (1) (2010) 17–31.

[31] ASHRAE, 2019 ASHRAE Handbook: HVAC Applications. Chapter 43: Supervisory control strategies and optimization, American Society of Heating Refrigerating and Air-Conditioning, 2019.

[32] M. Meyer, A. Emery, Optimal sizing and control of ice storage and refrigeration systems in commercial buildings, American Council for an Energy-Efficient Economy (ACEEE): Summer study on energy efficiency in buildings 1 (1992) 1–181.

[33] A. Baniasadi, D. Habibi, W. Al-Saedi, M. A. Masoum, C. K. Das, N. Mousavi, Optimal sizing design and operation of electrical and thermal energy storage systems in smart buildings, Journal of Energy Storage 28 (2020) 101186.

[34] L. Urbanucci, F. D'Ettorre, D. Testi, A comprehensive methodology for the integrated optimal sizing and operation of cogeneration systems with thermal energy storage, Energies 12 (5) (2019) 875.

[35] H.-J. Chen, D. W. Wang, S.-L. Chen, Optimization of an ice-storage air conditioning system using dynamic programming method, Applied thermal engineering 25 (2-3) (2005) 461–472.

[36] Liu, Prototype Building Models- Medium Office, United States Department of Energy, 2016.

[37] U. B. of labor statistics (2021). [link].
URL https://www.bls.gov/cpi/data.htm

[38] 2021 discount rates (2021).
URL https://www.energy.gov/sites/default/files/2021-04/2021discountrates.pdf

[39] R. Z. Kurt Roth, J. Brodrick, Cool thermal energy storage, American Society of Heating, Refrigerating and Air-Conditioning Engineers 48 (2006) 94–96.

[40] K. H. Drees, J. E. Braun, Modeling of area-constrained ice storage tanks, HVAC&R Research 1 (2) (1995) 143–158.

[41] USDOE, EnergyPlus Engineering Reference, U.S. Department of Energy, 2013.